

Heat Transfer and Entropy Generation of Power-Law Fluids Natural Convection Inside Triangular Cavity; Effect of Angle and Type of Magnetic Field Applied

Authors

Mohammad Nemati^a
Mohammad Sefid^{a*}
Ali J. Chamkha^b

^a Department of Mechanical Engineering, Yazd University, Yazd, Iran

^b Faculty of Engineering, Kuwait College of Science and Technology, Doha District, 35004 Kuwait

ABSTRACT

In the present work, heat transfer and entropy generation due to the natural convection of Newtonian and non-Newtonian fluids in two types of shear thinning and shear thickening inside a right-triangular cavity under the effect of uniform and non-uniform magnetic field by multiple relaxation time lattice Boltzmann methods have been investigated. The aspect ratio of the cavity is variable and the magnetic field is applied from left to right and perpendicular to the gravity of the cavity. The present work is validated with previous references and results presented in the form of tables, diagrams and streamlines, isothermal lines, and entropy lines. The simulation is done by writing the computer code in the Fortran language. The effect of Rayleigh number, aspect ratio, power-law index of fluid, Hartmann number and angle, and type of magnetic field applied on fluid flow and heat transfer characteristics has been evaluated. The results show that in all cases, increasing the Hartmann number and fluid power-law index leads to a decrease in the strength of flow, heat transfer rate, and entropy generated and the percentage of this effect varies depending on the number of other variables. By applying a magnetic field non-uniformly, the flow strength and heat transfer rate can be increased to about 45% and 20%, respectively. At higher Hartmann numbers, the effect of changing the type of magnetic field applied is more pronounced. The angle of the magnetic field applied is a determinant parameter on the amount of heat transfer so that the average Nusselt number in the horizontal mode is on average 15% less than in the vertical mode. Increasing of power-law index dramatically reduces the magnetic field effect so that it is ineffective for the shear thickening fluid, the type of magnetic field applied. By increasing the Rayleigh number and the aspect ratio of the cavity, the flow strength and the rate of heat transfer increase and the effect of the magnetic field becomes more pronounced. This study can be useful in the optimal design of industrial and engineering equipment, including electronic coolers.

Article history:

Received : 16 September 2021

Accepted : 24 December 2021

Keywords: Natural Convection, Power-law Fluids, Non-Uniform Magnetic Field, Entropy Generation, Variable Aspect Ratio, , Triangular Cavity, MRT-LBM.

* Corresponding author: Mohammad Sefid
Department of Mechanical Engineering, Yazd University, Yazd, Iran
Email: mhsefid@yazd.ac.ir

1. Introduction

The study of electrically conductive fluid under the effect of the magnetic field has received much attention due to its wide utilization in various applications such as the polymer industry, refining of molten metals, cooling of electronic equipment and many other cases [1-3]. In the recent decade, the interest in studying the behavior of heat transfer processes in closed cavities under the influence of a magnetic field is increasing. The common denominator of all these studies is that the fluid experiences Lorentz force. This force affects the buoyancy flow and heat transfer field [4-6]. Toghraei [7] investigated the effect of a magnetic field on the flow characteristics of nanofluid mixed convection within the trapezoidal chamber at a different angle of inclination by the finite volume method using the simpler algorithm. Results showed that the heat transfer rate decreases with increasing Hartmann number and the average Nusselt number is a function of the Reynolds number and the angle of inclination of the chamber. The natural convection of the non-Newtonian fluid under the effect of a uniform magnetic field in a square-shaped chamber was studied by Kefayati and Tang [8]. For electrically conductive fluids, the Lorentz force due to the application of a magnetic field reduces the velocity of the fluid. This phenomenon has led to the use of magnetic fields to control the flow and rate of heat transfer in the industry. The directions and strength of the magnetic field play a very important role in the behavior of the current [9]. The unwanted magnetic field is not always uniform. Sometimes it is necessary to apply a non-uniform magnetic field in order to achieve a specific goal. For this reason, it is important to study the heat transfer flows affected by a non-uniform magnetic field. Most studies have examined the study of displacement currents under a uniform magnetic field. Nemati et al. [10] investigated the mixed convection within a porous chamber by moving the walls in different directions due to uniform/periodic magnetic field and heat generation/ absorption by the Boltzmann lattice method. The results showed that by periodically applying the magnetic field compared to the uniform state, the flow strength and the average Nusselt

number are higher and the highest heat transfer rate was observed for the two oscillation waves.

The entropy generated according to the second law of thermodynamics can be a measure of equipment efficiency. For this reason, in recent years, in addition to studying heat transfer, researchers have also been evaluating the amount of entropy produced [11]. Entropy generation reduces thermodynamic efficiency. Entropy analysis shows in which parts of a physical model or system the energy dissipation is greater [12]. Since the production of entropy is a criterion for the loss of workability in equipment, it is necessary to determine the issue of increasing the efficiency of devices [13-15].

The fluids used in real applications have Newtonian and non-Newtonian properties, so it is important to study the flow characteristics and heat transfer properties created by non-Newtonian fluids [16]. Unlike Newtonian fluids, in non-Newtonian fluids, a constant coefficient such as viscosity does not make sense to describe the state of shear stress [17]. Most fluids used in the mechanical and chemical industries are non-Newtonian [18]. Non-Newtonian fluid streams have been used in many natural and industrial applications, including industrial product lines, and polymer processes, and in many biological applications such as blood flow in the body [19-21].

Natural convection is one of the heat transfer processes and occurs when a volumetric force is applied to it by creating a density difference due to the temperature difference in the fluid [22]. Heat transfer in closed cavities has a variety of applications in industry, including applications in electric machines, microelectronic devices and solar collectors. Therefore in designing all these types of equipment, simulation of heat transfer in the cavity with different shapes can be useful and necessary [23].

Today, the lattice Boltzmann method is a numerical method based on the theory of molecular motion that is widely used in simulating transfer phenomena. Features of this method include simple application of boundary conditions, parallelism and application in solving complex problems such as combustion simulation [24-26]. The multi-relaxation time lattice Boltzmann method (MRT-LBM) has

more stability and degree of freedom than the Single relaxation Time (SRT-LBM).

Rahman et al. [27] investigated the natural convection of a non-Newtonian fluid in a rectangular cavity in the presence of a uniform magnetic field by the multi relaxation time lattice Boltzmann method. The results showed that the use of MRT-LBM has a high accuracy in heat transfer simulation and the results have an acceptable agreement with other methods. They also indicated that the average Nusselt number and the entropy generated obviously depend on the Rayleigh number, the Hartmann number, and the power-law index. Jahanbakhshi et al. [28] investigated the heat transfer of a non-Newtonian fluid with a power-law model under the effect of a uniform magnetic field with the simple algorithm and the finite volume method inside the L-shaped cavity. Afsana et al. [29] evaluated the non-Newtonian fluid natural convection with a power-law model inside a square cavity with corrugated walls in the presence of a uniform magnetic field by the finite volume method. The results showed that the amount of heat transfer is clearly dependent on Rayleigh number, Hartmann number and power index and the average Nusselt number decreases with increasing power index. Also, the increment of Hartmann number results in 60% attenuation of total entropy for shear-thinning fluid and 9% diminution for the shear-thickening case. In addition, the effect of increasing the Hartmann number on reducing the total entropy generation for the shear thinning fluid is greater than shear thickening fluid. Zhang et al. [30] investigated the heat transfer and entropy generation due to the natural convection of Newtonian and non-Newtonian fluids in an L-shaped chamber numerically under the influence of a magnetic field. The results showed that the average Nusselt number and total entropy generation increased with increasing Rayleigh number and decreased with increasing power-law index and Hartmann number. Rahimi et al. [31] used the lattice Boltzmann method to investigate heat transfer and entropy generation of nanofluid in an H-shaped chamber. The results showed that the total entropy and average Nusselt number are a function of Riley number and nanoparticle volume fraction.

According to previous studies, it has been seen that the heat transfer and entropy

generated due to natural convection inside the triangular cavity under the effect of uniform and non-uniform magnetic fields (specific type of applied) have not been studied so far. A feature of the present work is the application of the multi relaxation time lattice Boltzmann method (MRT-LBM) to solve this study which has not been done before.

List of symbols

AR	Aspect ratio
B	Strength of magnetic field
Be	Bejan number
c	Discrete particle speeds for D_2Q_6
e	Discrete particle speeds for D_2Q_8
f	Functions of density distribution
f^{eq}	Equilibrium density distribution functions
F	External force
g	Acceleration due to gravity
h	Internal energy distribution functions
h^{eq}	Equilibrium internal energy distribution functions
H	Height of the cavity
Ha	Hartmann number
k	Coefficient of thermal conductivity
L	Length of the cavity
n	Index of power-law
Nu	Nusselt number
Pr	Prandtl number
Ra	Rayleigh number
T	Temperature
S	Entropy generation
u (u,v)	Velocities
x (x,y)	Cartesian coordinates
α	Thermal diffusivity
λ	Angle of magnetic field applied
μ	Dynamic viscosity
ν	Kinematic viscosity
ψ	Stream function
ω	Weighting factor
θ	Dimensionless temperature

2. Description of the present problem

In the present work, the heat transfer and entropy generated due to the natural convection of Newtonian and non-Newtonian power-law

fluids (shear thinning and shear thickening) are inside a triangular cavity with variable aspect ratio investigated. The diagonal wall of the cavity is at a constant cold temperature while the vertical wall has a sinusoidal temperature distribution. Also, the horizontal wall is considered adiabatic. Magnetic field with different powers is applied in two types of uniform and non-uniform (In four different forms) from left to right and perpendicular to the gravity on the cavity. The schematic of this problem is shown in Fig. 1. Fig. 2 shows an example of the computational network used in the present study. Table 1 presents the studied parameters in this along with the corresponding values. . All flow boundaries are impenetrable and there is no slippage on the surfaces. The fluid flow is steady and laminar and the Boussinesq approximation is used. Viscous loss and radiative heat transfer are negligible.

3. Governing equations

Assuming that the flow fluid is incompressible and using the Boussinesq approximation, the equations of mass, momentum and energy are presented in Eqs. (1) to (4) [30]. Stream function is defined as relation (5). The dynamic viscosity in the power-law model is defined as Eq. (6) [27]. Total generated entropy is the sum of the generated entropies due to heat transfer, fluid friction and magnetic field that it is expressed according to relation (6) to (10). The power-law index of the fluid is indicated by n and in the case of a Newtonian fluid is $n = 1$, $n < 1$ indicates shear thinning fluid and $n > 1$ indicates shear thickening fluid. By using dimensionless parameters in relation (11), the governing equations are written as relations (12) to (21).

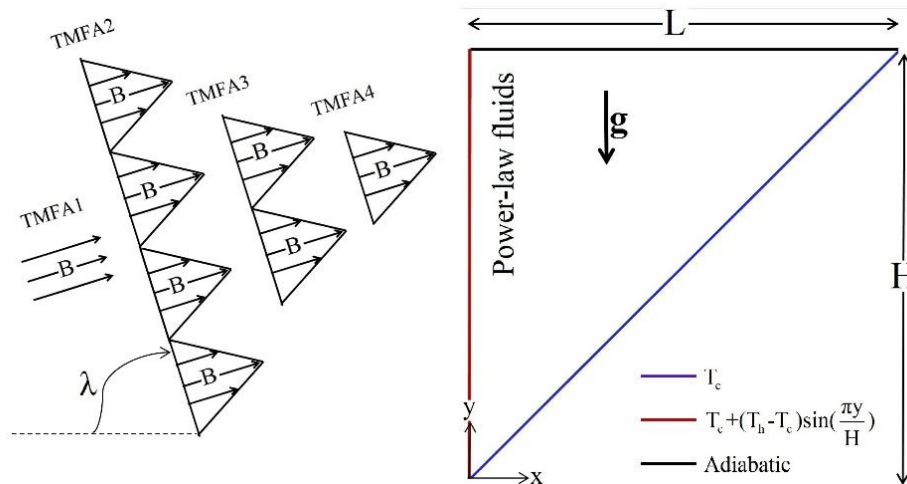


Fig. 1. Geometry of the present problem

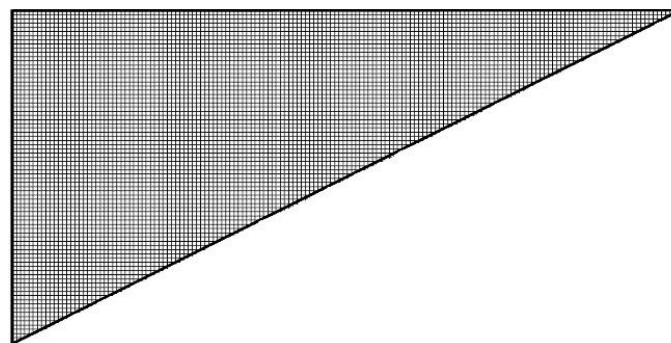


Fig. 2. Representation of the grid distribution

Table 1. Dimensionless parameters used in the present work

Dimensionless parameters	Values
Hartmann number	0, 15, 30 and 45
Type of magnetic field applied	TMFA1, TMFA2, TMFA3 and TMF4
Angle of magnetic field applied	0 and 90°
Rayleigh number	10 ³ , 10 ⁴ and 10 ⁵
Aspect ratio of cavity (AR=L/H)	0.5, 1 and 2
Power-law index	0.75, 1.0 and 1.25

$$\frac{\partial u}{\partial x} + \frac{\partial v}{\partial y} = 0 \tag{1}$$

$$\rho(u \frac{\partial u}{\partial x} + v \frac{\partial u}{\partial y}) = -\frac{\partial p}{\partial x} + \frac{\partial}{\partial x}(2\mu \frac{\partial u}{\partial x}) + \frac{\partial}{\partial y}(\mu \frac{\partial u}{\partial y}) + \frac{\partial}{\partial y}(\mu \frac{\partial v}{\partial x}) + \sigma B^2(v \sin \lambda \cos \lambda - u \cos^2 \lambda) \tag{2}$$

$$\rho(u \frac{\partial v}{\partial x} + v \frac{\partial v}{\partial y}) = -\frac{\partial p}{\partial y} + \frac{\partial}{\partial x}(\mu \frac{\partial v}{\partial x}) + \frac{\partial}{\partial y}(2\mu \frac{\partial v}{\partial y}) + \frac{\partial}{\partial x}(\mu \frac{\partial u}{\partial y}) + \rho \beta g \theta + \sigma B^2(u \sin \lambda \cos \lambda - v \sin^2 \lambda) \tag{3}$$

$$u \frac{\partial T}{\partial x} + v \frac{\partial T}{\partial y} = \alpha (\frac{\partial^2 T}{\partial x^2} + \frac{\partial^2 T}{\partial y^2}) \tag{4}$$

$$\psi(x,y) = \int u dy + \psi_0 \tag{5}$$

$$\mu = \mu_0 \left\{ 2 \left[\left(\frac{\partial u}{\partial x} \right)^2 + \left(\frac{\partial v}{\partial y} \right)^2 \right] + \left(\frac{\partial v}{\partial x} + \frac{\partial u}{\partial y} \right)^2 \right\}^{\frac{(n-1)}{2}} \tag{6}$$

$$S = S_T + S_F + S_M \tag{7}$$

$$S_T = \frac{k}{T_0^2} \left[\left(\frac{\partial T}{\partial x} \right)^2 + \left(\frac{\partial T}{\partial y} \right)^2 \right] \tag{8}$$

$$S_F = \frac{\mu \gamma}{T_0} \left[2 \left(\left(\frac{\partial u}{\partial x} \right)^2 + \left(\frac{\partial v}{\partial y} \right)^2 \right) + \left(\frac{\partial v}{\partial x} + \frac{\partial u}{\partial y} \right)^2 \right] \tag{9}$$

$$S_M = \frac{\sigma B^2}{T_0} (u \sin \lambda - v \cos \lambda)^2 \tag{10}$$

In above relation, S_F, S_H and S_M represents the entropy generated due to fluid friction, heat transfer and magnetic field, respectively and $T_0 = \frac{T_h + T_c}{2}$.

$$X = \frac{x}{H}, Y = \frac{y}{H}, U = \frac{uH}{\alpha \sqrt{Ra}}, V = \frac{vH}{\alpha \sqrt{Ra}}, v_0 = \frac{\mu_0}{\rho}, Pr = \frac{v_0 H^{2-n}}{\alpha^{2-n}}, \theta = \frac{T - T_c}{T_h - T_c}, Ha = BH^n \sqrt{\frac{\sigma \alpha^{1-n}}{\mu_0}}, Ra = \frac{\beta \theta g H^{2n+1}}{v_0 \alpha^n}, P = \frac{pH^2}{\rho R \alpha^2}, \alpha = \frac{v_0}{Pr} \tag{11}$$

$$\frac{\partial U}{\partial X} + \frac{\partial V}{\partial Y} = 0 \tag{12}$$

$$U \frac{\partial U}{\partial X} + V \frac{\partial U}{\partial Y} = -\frac{\partial P}{\partial X} + \frac{Pr Ha^2}{\sqrt{Ra}} (V \sin \lambda \cos \lambda - U \cos^2 \lambda) + \frac{Pr}{Ra^{\frac{(2-n)}{2}}} \left[\frac{\partial}{\partial X} (2\chi \frac{\partial U}{\partial X}) + \frac{\partial}{\partial Y} (\chi \frac{\partial U}{\partial Y}) + \frac{\partial}{\partial Y} (\chi \frac{\partial V}{\partial X}) \right] \tag{13}$$

$$U \frac{\partial V}{\partial X} + V \frac{\partial V}{\partial Y} = -\frac{\partial P}{\partial Y} + Pr \theta + \frac{Pr Ha^2}{\sqrt{Ra}} (U \sin \lambda \cos \lambda - V \sin^2 \lambda) + \frac{Pr}{Ra^{\frac{(2-n)}{2}}} \left[\frac{\partial}{\partial X} (\chi \frac{\partial V}{\partial X}) + \frac{\partial}{\partial Y} (2\chi \frac{\partial V}{\partial Y}) + \frac{\partial}{\partial X} (\chi \frac{\partial U}{\partial Y}) \right] \tag{14}$$

$$U \frac{\partial \theta}{\partial X} + V \frac{\partial \theta}{\partial Y} = \frac{1}{\sqrt{Ra}} \left(\frac{\partial^2 \theta}{\partial X^2} + \frac{\partial^2 \theta}{\partial Y^2} \right) \tag{15}$$

$$\Psi(X,Y) = \int U dY + \Psi_0 \tag{16}$$

$$\chi = |\gamma|^{(n-1)} = \left\{ 2 \left[\left(\frac{\partial U}{\partial X} \right)^2 + \left(\frac{\partial V}{\partial Y} \right)^2 \right] + \left(\frac{\partial V}{\partial X} + \frac{\partial U}{\partial Y} \right)^2 \right\}^{\frac{(n-1)}{2}} \tag{17}$$

$$S = S_T + S_F + S_M \tag{18}$$

$$S_T = \left[\left(\frac{\partial \theta}{\partial X} \right)^2 + \left(\frac{\partial \theta}{\partial Y} \right)^2 \right] \tag{19}$$

$$S_F = \eta_1 \chi \left[2 \left(\left(\frac{\partial U}{\partial X} \right)^2 + \left(\frac{\partial V}{\partial Y} \right)^2 \right) + \left(\frac{\partial U}{\partial Y} + \frac{\partial V}{\partial X} \right)^2 \right] \tag{20}$$

$$S_M = \eta_2 Ha^2 (U \sin \lambda - V \cos \lambda)^2 \tag{21}$$

According to references [32-34] in the present work, η_1 and η_2 is considered to be 10^{-4} .

The total entropy generation value is on averaged according to relation (22). The Bejan number (Be) which represents the ratio of the entropy generation due to heat transfer to the total entropy generation is calculated according to relation (23). $Be > 0.5$ indicates the dominance of irreversibility due to heat transfer to other irreversibility, including friction and magnetic field. The average Nusselt number (Nu) which is a measure of heat transfer on the hot wall of a cavity is defined as Eq. (24).

$$S = \frac{\int_{\partial V} s d\bar{V}}{\bar{V}} \quad (22)$$

$$Be = \frac{S_T}{S} \quad (23)$$

$$Nu = \frac{1}{H} \int_0^1 -\left(\frac{\partial \theta}{\partial X}\right)_{X=0} dY \quad (24)$$

The non-Newtonian fluid studied in the present work follows the power-law model. In this model, the kinematic viscosity is a function of the shear rate that is defined as a relation (25) and (26). The kinematic viscosity of a non-Newtonian fluid is expressed according to equation (27).

$$\gamma_{ij} \equiv 0.5 \left(\frac{\partial u_i}{\partial x_j} + \frac{\partial u_j}{\partial x_i} \right) \quad (25)$$

$$|\gamma| = \sqrt{2\gamma_{ij}\gamma_{ij}} \quad (26)$$

$$v(\mathbf{x}, t) = v_0 |\gamma|^{(n-1)} = \frac{Pr}{Ra^{\frac{(2-n)}{2}}} |\gamma|^{(n-1)} \quad (27)$$

4. Numerical method

In the present work, the lattice Boltzmann method with multiple relaxation time (MRT) in the collision stage has been used. The advantage of this method over the single relaxation time (SRT) is higher accuracy and stability. For the flow field, the D_2Q_9 lattice arrangement is used as shown in Fig. 3. The lattice Boltzmann equation is presented in Eq. (28).

$$f_i(\mathbf{x} + \mathbf{c}_i, t+1) = f_i(\mathbf{x}, t) - \Omega [f_i(\mathbf{x}, t) - f_i^{eq}(\mathbf{x}, t)] + \mathbf{c}_i \mathbf{F}_i(\mathbf{x}, t) \quad (28)$$

In the above relation, f is the distribution function, Ω is the collision matrix and \mathbf{F}_i denotes components the body forces. Equilibrium distribution functions is calculated according to Eq.(29). In the D_2Q_9 lattice arrangement model, the weighting factor and discrete velocity are expressed according to Eqs. (30) and (31), respectively.

$$f_i^{eq} = \rho \omega_i^f \left[1 + 3(\mathbf{c}_i \cdot \mathbf{u}) - \frac{3}{2}(\mathbf{u} \cdot \mathbf{u}) + 4.5(\mathbf{c}_i \cdot \mathbf{u})^2 \right] \quad (29)$$

$$\omega_0^f = \frac{4}{9}, \omega_{1-4}^f = \frac{1}{9}, \omega_{5-8}^f = \frac{1}{36} \quad (30)$$

$$\mathbf{c}_0 = 0$$

$$\mathbf{c}_{1-4} = \left[\cos\left(\frac{(i-1)\pi}{2}\right), \sin\left(\frac{(i-1)\pi}{2}\right) \right] \quad (31)$$

$$\mathbf{c}_{5-8} = \sqrt{2} \left[\cos\left(\frac{(i-5)\pi}{2} + \frac{\pi}{4}\right), \sin\left(\frac{(i-5)\pi}{2} + \frac{\pi}{4}\right) \right]$$

After performing the collision process in the momentum space instead of the velocity space, the equation yields to:

$$\begin{aligned} f_i(\mathbf{x} + \mathbf{c}_i, t+1) &= f_i(\mathbf{x}, t) - \\ &\mathbf{M}^{-1} \mathbf{S} \left[\mathbf{m}(\mathbf{x}, t) - \mathbf{m}^{eq}(\mathbf{x}, t) \right] + \mathbf{M}^{-1} \left(\mathbf{I} - \frac{\mathbf{S}}{2} \right) \mathbf{F}(\mathbf{x}, t) \\ \mathbf{f} &= (f_0, f_1, \dots, f_9)^T \\ \mathbf{m} &= (m_0, m_1, \dots, m_9)^T \\ \mathbf{F} &= (F_0, F_1, \dots, F_9)^T \end{aligned} \quad (32)$$

In the above equation \mathbf{M} is the transformation matrix that transfers the vector of the distribution function to the momentum space. For D_2Q_9 model, \mathbf{M} is according to relation (33).

$$\mathbf{M} = \begin{bmatrix} 1 & 1 & 1 & 1 & 1 & 1 & 1 & 1 & 1 \\ -4 & -1 & -1 & -1 & -1 & 2 & 2 & 2 & 2 \\ 4 & -2 & -2 & -2 & -2 & 1 & 1 & 1 & 1 \\ 0 & 1 & 0 & -1 & 0 & 1 & -1 & -1 & 1 \\ 0 & -2 & 0 & 2 & 0 & 1 & -1 & -1 & 1 \\ 0 & 0 & 1 & 0 & -1 & 1 & 1 & -1 & -1 \\ 0 & 0 & -2 & 0 & 2 & 1 & 1 & -1 & -1 \\ 0 & 1 & -1 & 1 & -1 & 0 & 0 & 0 & 0 \\ 0 & 0 & 0 & 0 & 0 & 1 & -1 & 1 & -1 \end{bmatrix} \quad (33)$$

The diagonal matrix \mathbf{S} is the collision matrix in a moment space that is presented in relation (34).

$$\mathbf{S} = \text{diag}\left(1, 1.4, 1.4, 1.2, 1, 1.2, \frac{1}{\tau_1}, \frac{1}{\tau_1}\right) \quad (34)$$

In the above relation: $\tau_1=3v(\mathbf{x},t)+0.5$. Eqs. (35) and (36) present the moment (m) and equilibrium moment (m^{eq}) vectors. In relation (28), \mathbf{F} represents the total volumetric forces and is written as relation (37) [27].

$$m=\mathbf{M}f \tag{35}$$

$$\begin{aligned} m_0^{eq} &= \rho, m_1^{eq} = -2\rho + 3(j_x^2 + j_y^2), m_2^{eq} = \rho - 3(j_x^2 + j_y^2), m_3^{eq} = j_x, \\ m_4^{eq} &= -j_x, m_5^{eq} = j_y, m_6^{eq} = -j_y, m_7^{eq} = (j_x^2 - j_y^2), m_8^{eq} = (j_x - j_y) \end{aligned} \tag{36}$$

In the above relation: $j_x = \rho u, j_y = \rho v$. In relation (28), \mathbf{F} represents the total volumetric forces and is written as relation (37) [27].

$$\mathbf{F} = \mathbf{F}_x + \mathbf{F}_y$$

$$F_x = 3\omega_f^f \rho \frac{Ha^2 v(\mathbf{x}, t)}{H^2} (v \sin \lambda \cos \lambda - u \sin^2 \lambda) \tag{37}$$

$$F_y = 3\omega_f^f \rho \frac{Ha^2 v(\mathbf{x}, t)}{H^2} (u \sin \lambda \cos \lambda - v \cos^2 \lambda) + 3\omega_f \rho g \beta \theta$$

The macroscopic fluid density (ρ) and velocity \mathbf{u} are obtained from the moments of the distribution function given below:

$$\rho = \sum_{i=0}^8 f_i, \mathbf{u}(x, y) = \frac{1}{\rho} \sum_{i=0}^8 \mathbf{c}_i f_i \tag{38}$$

Like the flow field, the MRT-LBM and the D_2Q_5 lattice arrangement are used to solve the temperature field, the equation of which is presented in Eqs. (39) to (41) [27,35]. A schematic of this type of lattice arrangement is shown in Fig. 3.

$$h_i(\mathbf{x} + \mathbf{e}_i, t + 1) = h_i(\mathbf{x}, t) - \mathbf{N}^{-1} \mathbf{Z} \cdot [n(\mathbf{x}, t) - n^{eq}(\mathbf{x}, t)] \tag{39}$$

$$n = \mathbf{N}h \tag{40}$$

$$n_0^{eq} = T, n_1^{eq} = uT, n_2^{eq} = vT, n_3^{eq} = \left(\frac{60\alpha}{\sqrt{3}} - 4\right)T, n_4^{eq} = 0 \tag{41}$$

In relation (39), h is the distribution function of the temperature field ($h=(h_0, h_1, h_2, h_3, h_4)^T$). \mathbf{e} is the microscopic velocity of the particles in the D_2Q_5 lattice arrangement presented in Eq. (42).

$$\mathbf{e}_0 = 0, \mathbf{e}_1 = (1, 0), \mathbf{e}_2 = (0, 1), \mathbf{e}_3 = (-1, 0), \mathbf{e}_4 = (0, -1) \tag{42}$$

The \mathbf{N} and \mathbf{Z} collision matrices are in the form of relations (43) and (44).

$$\mathbf{N} = \begin{bmatrix} 1 & 1 & 1 & 1 & 1 \\ 0 & 1 & 0 & -1 & 0 \\ 0 & 0 & 1 & 0 & -1 \\ -4 & 1 & 1 & 1 & 1 \\ 0 & 1 & -1 & 1 & -1 \end{bmatrix} \tag{43}$$

$$\mathbf{Z} = \text{diag}(1, z_\alpha, z_\alpha, z_e, z_v) \tag{44}$$

In the above relation:

$$\frac{1}{z_\alpha} - 0.5 = \frac{1}{z_e} - 0.5 = \frac{1}{6}, \frac{1}{z_v} - 0.5 = \frac{\sqrt{3}}{6} \tag{45}$$

The equilibrium distribution function and the macroscopic quantities related to the temperature field are calculated using Eqs. (46) and (47), respectively.

$$h_i^{eq} = \omega_i^h T [1 + 3(\mathbf{c}_i \cdot \mathbf{u})] \tag{46}$$

$$T = \sum_{i=0}^8 h_i \tag{47}$$

Which $\omega_0^h = 0, \omega_{1-4}^h = 0.25$ is for the D_2Q_5 model. The vertical and diagonal walls of the cavity are at a constant hot and cold

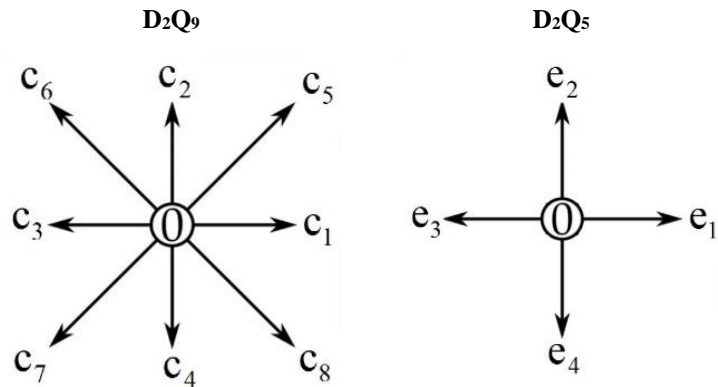


Fig. 3. Lattice arrangement

temperature, respectively. While the top horizontal wall considered adiabatic. Mathematical relations of the boundary conditions of the present problem are in the form of relation (48).

$$\begin{aligned} \text{Hot wall : } & U=V=0, \theta=1, \\ \text{Cold wall : } & U=V=0, \theta=0, \\ \text{Adiabatic wall : } & U=V=0, \frac{\partial \theta}{\partial Y}=0 \end{aligned} \quad (48)$$

It is necessary to mention that in this simulation, the bounce-back model is used to the simulation of the boundary conditions on smooth and diagonal walls. Details and related relationships are listed in references such as [36-38].

Choosing the right algorithm to solve the problem and achieve the correct results is very important. First, the initial parameters such as Prandtl number, Rayleigh number and initial distribution functions are considered. Then, according to Eqs. (29) and (46), the values of equilibrium distribution functions in fluid nodes are calculated. In the collision step, relations (28) and (39) are satisfied and then the new values of the distribution functions (after the collision) are calculated. Then the streaming step is performed when the values of the distribution functions of all nodes in their direction are poured on adjacent nodes. After applying the boundary conditions, the values of density, velocity and temperature in the whole network are calculated according to Eqs. (38) and (47). Finally, the shear rate is calculated in all nodes and if the results converge, the program ends, otherwise, the described steps will be repeated.

Convergence relationship for completing calculations in order to save time and cost and to have the necessary accuracy in relation (49) provided.

$$\text{Error} = \frac{\sum_{i=1}^{f_1} \sum_{j=1}^{f_2} |\Gamma^{b+1} - \Gamma^b|}{\sum_{i=1}^{f_1} \sum_{j=1}^{f_2} |\Gamma^b|} \leq 10^{-8} \quad (49)$$

In above relation, b and $b+1$ represent the old and new time phases and r_1 and r_2 represent the number of nodes in the x and y directions, respectively. The parameter Γ stands for U , V or θ .

5. Validations and grid independence study

One of the requirements of numerical simulation is validation with previous reliable studies. For this purpose, the present work is the comparison with several references and its results are presented. In order to validate the written code in calculating the entropy generated, the present work is compared with the reference [39] in Fig. 4. Also, the correctness of the computer program in simulating the heat transfer of non-Newtonian fluid with the power-law model in the presence of magnetic field according to Fig. 5 (comparison of the present work with the reference [36]) is shown. In addition, a comparison of the average Nusselt number on the hot wall of the cavity between the present work and the reference [40] and [41] for natural convection of non-Newtonian fluid is presented in Table 2.

The very small difference between the results obtained from the present code and the results of previous studies indicates the correctness of the written program in Fortran language.

To obtain a suitable lattice that leads to the independence of the results from the selected network, the lattice with dimensions of 40×80 , 60×120 , 80×160 , 100×200 and 120×240 was selected. According to Table 3, it can be seen that for a network with dimensions larger than 100×100 , no significant change is seen in the results and the accuracy of the results can be ensured.

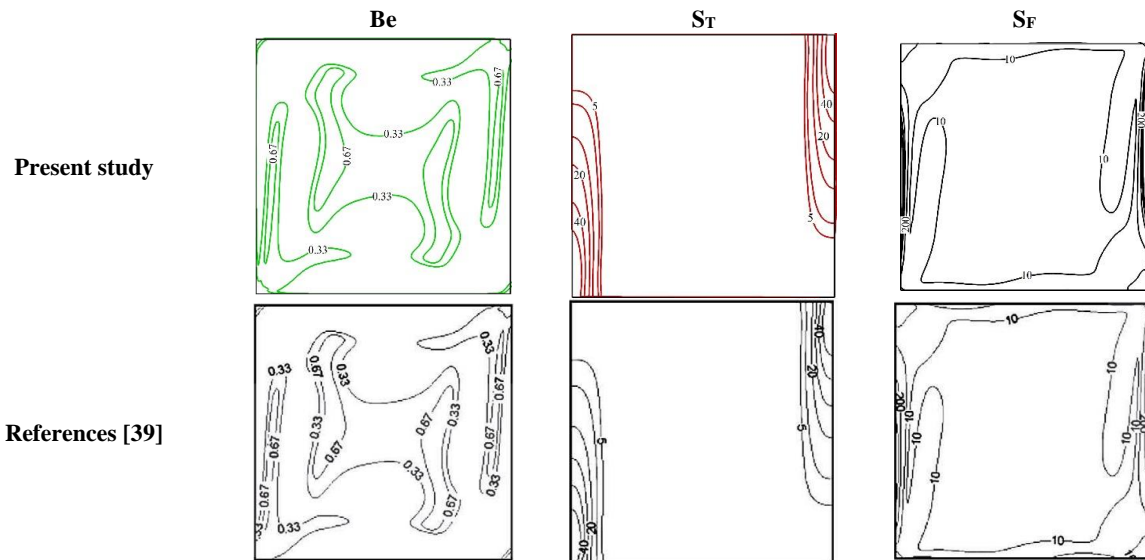


Fig. 4. Comparison between the present study and reference [39]

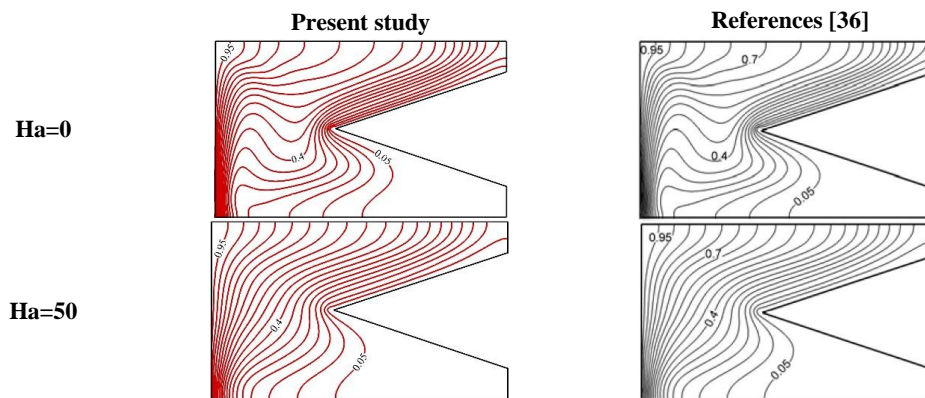


Fig. 5. Comparison between the present study and reference [36]

Table 2. Comparison between present study and reference [40] and [41]

	Ra=10 ⁴			Ra=10 ⁵		
	Reference [40]	Reference [41]	Present study	Reference [40]	Reference [41]	Present study
n=0.7	1.03	1.04	1.04	1.3	1.32	1.31
n=0.9	1.01	1.02	1.02	1.09	1.1	1.1
n=1.0	1.0	1.0	1.0	1.05	1.05	1.05
n=1.1	0.99	0.98	0.975	0.93	0.92	0.92
n=1.3	0.95	0.94	0.94	0.86	0.85	0.85

Table 3. Average Nusselt number for different mesh size at AR=2, λ=90°, Ha=15, TMFA1 and Ra=10⁵

	Mesh size	40×80	60×120	80×160	100×200	120×240
n=0.75	Nu	5.331	7.535	7.715	7.831	7.897
	Error	-	3.82	2.38	1.51	0.85
	Ψ _{max}	0.305	0.315	0.345	0.357	0.368
n=1.25	Nu	5.099	5.208	5.287	5.351	5.2351
	Error	-	2.08	1.51	0.012	0
	Ψ _{max}	0.096	0.099	0.105	0.105	0.105

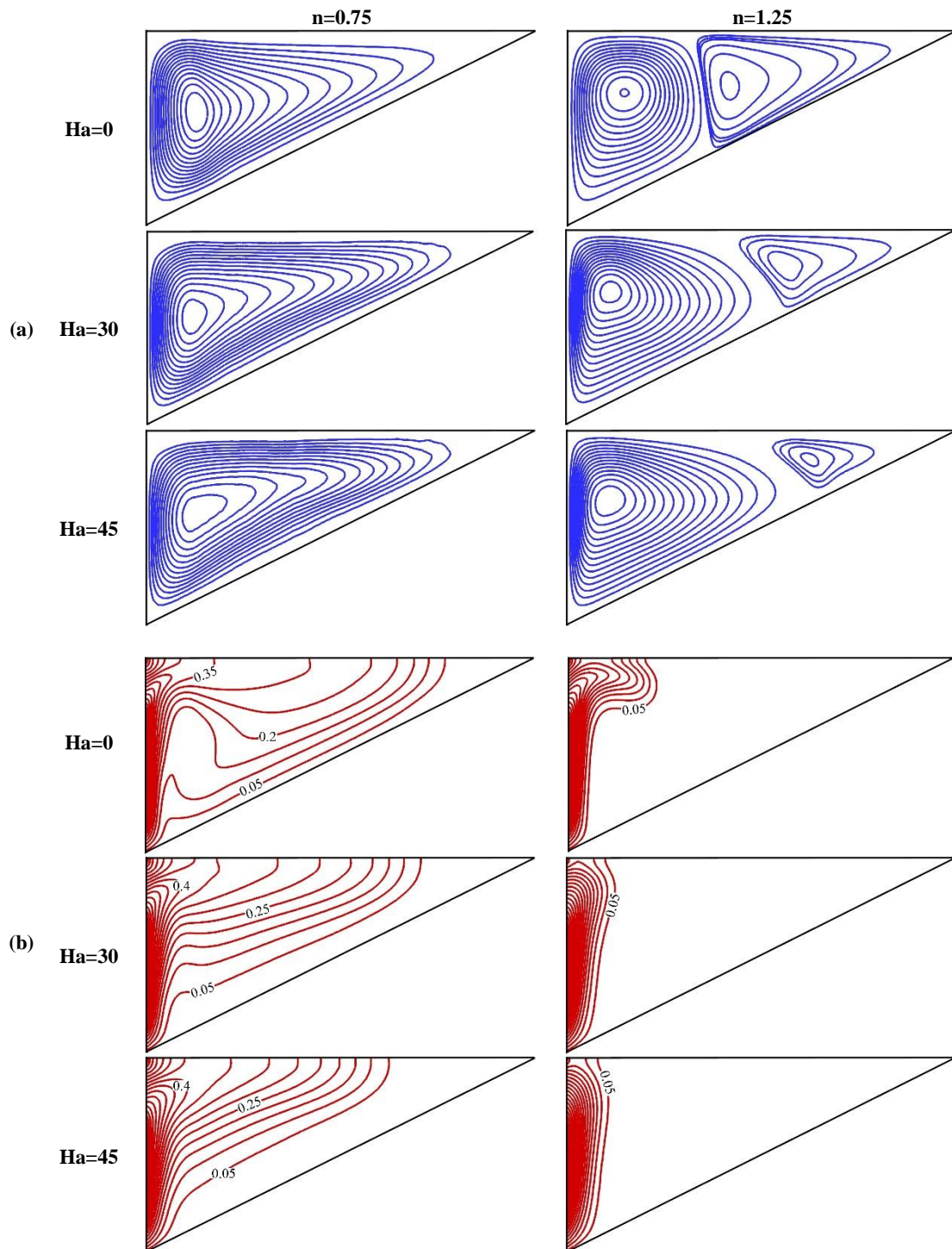
5. Results and discussion

In this section, the results of simulations are presented and analyzed for variations in Rayleigh number, Hartmann number, power-law index, the aspect ratio of cavity, angle and type of magnetic field applied (Table 1). The results are presented in the form of tables, diagrams and contours of streamlines, isothermal lines, and constant entropy lines. Since the non-Newtonian fluids used in industry have large Prandtl numbers, in the present work, $Pr=100$ has been chosen.

5.1. Effect of magnetic field

Figure 6 shows contours of streamlines, isotherms, and local entropy generation due to heat transfer at different values of the Hartmann number for shear thickening and shear thinning fluid. According to Fig. 6 (a), in all cases, the fluid heats up near the hot vertical wall and moves upwards due to the decrease in density and then its density increases in contact with the cold wall, which leads to the formation of a clockwise vortex in the cavity. When the fluid has a shear thickening behavior, due to the high viscosity of the fluid, a vortex with less strength is formed in the right corner of the cavity. Increasing the Hartmann number causes the center of the vortices to shift upwards because the magnetic field acts against gravity. According to Fig. 6 (b) it can be seen that the scattering of isotherms for the shear thickening fluid is much less compared to the shear thinning fluid and the lines are densely adjacent to the hot wall and show that thermal conductivity is the predominant heat transfer phenomenon. Because according to Eq. (27), increasing the power-law index increases the viscosity of the fluid and reduces the effects of convection. Increasing the Hartmann number in both non-Newtonian fluid behaviors reduces the curvature and dispersion of the isotherms. Because according to Eqs. (2) and (3), increasing the Hartmann number leads to an increase in Lorentz force in the opposite direction of gravity force that reduces the velocity of the fluid. Due to the greater convection effects for shear thinning fluid compared to the shear thickening fluid, the

effect of the magnetic field for the shear thinning fluid is more obvious. According to Fig. 1 (c), it can be seen that the constant entropy lines due to heat transfer behave similarly to isotherms so that the generated entropy decreases with increasing Hartmann number and power-law index. Due to the higher temperature and velocity gradient adjacent to the hot wall, the highest entropy generated is observed in this area. The horizontal velocity for the different values of the power-law index and the Hartmann number is shown in Fig. 7. It can be seen that the velocity of the fluid decreases with increasing power-law index and Hartmann number. The effect of increasing the strength of the magnetic field on decreasing the velocity decreases with increasing the power-law index. Because increasing the power-law index causes the heat transfer mechanism to be inclined towards conduction. According to Table 4, the strength of flow in all cases decreases with increasing Hartmann number. Because increasing the Lorentz force reduces the velocity of the flow. Also, it can be seen that when the magnetic field is applied horizontally, the strength of flow decreases more because according to Eqs. (2) and (3), when the magnetic field is applied horizontally, the Lorentz force acts against gravity. By applying the magnetic field horizontally, the strength of flow was reduced by an average of 20%. As the power-law index increases, the strength of flow decreases and the effect of the magnetic field decreases.



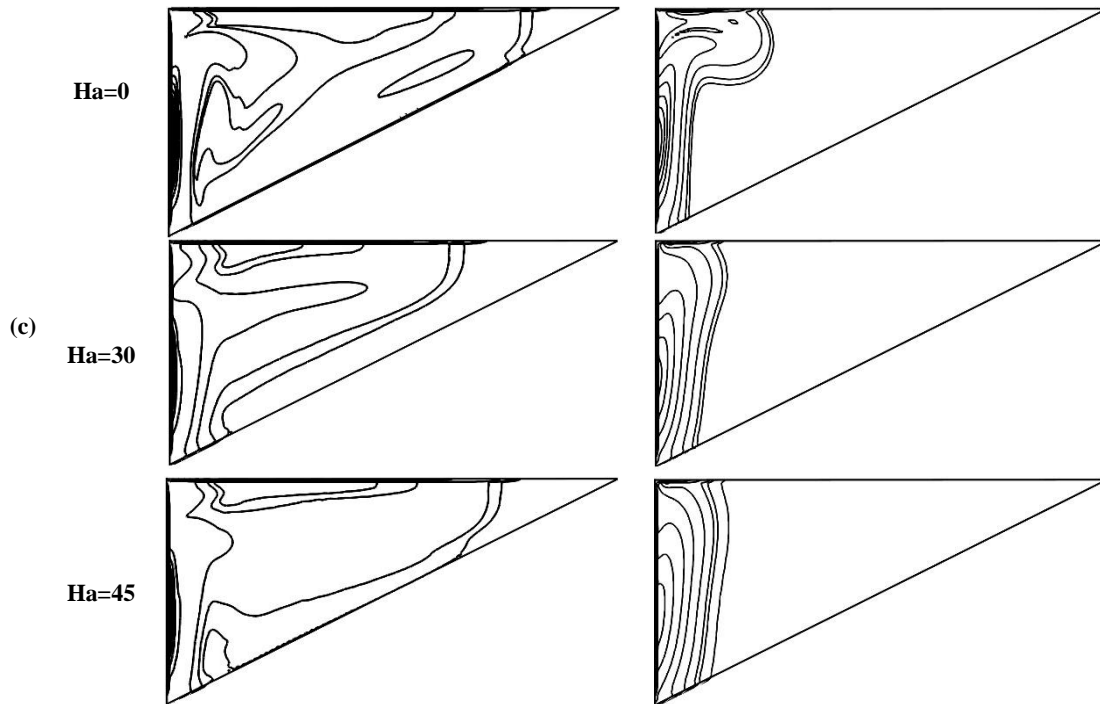


Fig. 6. Contours of (a) streamlines, (b) isotherms and (c) entropy generation due to heat transfer for various Hartmann numbers in shear thickening and shear thinning fluid at $AR=2$, $Ra=10^5$, $\lambda=90^\circ$ and TMFA1

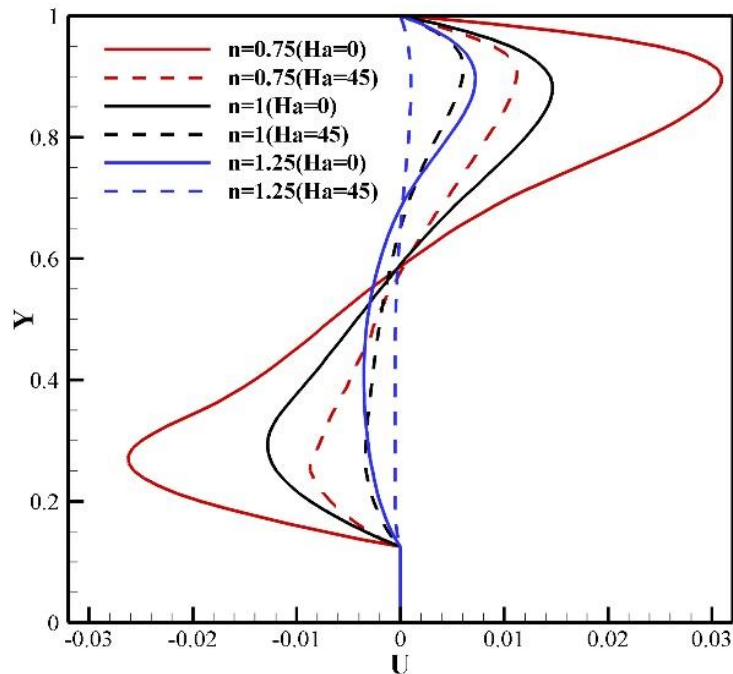


Fig. 7. Horizontal velocity in $X=0.25$ for variations of rheological behavior of fluid and Hartmann number at $AR=2$, $Ra=10^5$, $\lambda=90^\circ$ and TMFA1

The average Nusselt number and the volumetric total entropy generation for different values of the Hartmann numbers, the fluid power-law index, and the angle of the magnetic field applied are shown in Fig. 8. It can be seen that in all values of Hartmann number, the maximum and minimum values of the average Nusselt number are related to shear thinning and shear thickening fluid, respectively. Increasing the power-law index according to Eq. (27) leads to increasing the viscosity of the fluid and as a result the power of fluid and velocity of the fluid decreases according to Fig. 6 (b), because the thermal conductivity prevails, the rate of heat transfer become decreases. The percentage decrease of the average Nusselt number is higher with the increase of the Hartmann number in the case where the magnetic field is horizontally applied. On average, increasing the Hartmann number from zero to 45 leads to a 35, 28, and 17 percent decrease in the average Nusselt number for shear thinning, Newtonian, and shear thickening fluids, respectively. The trend of total entropy generation variations is similar to the average Nusselt number changes. This shows that the largest share of the total entropy belongs to the entropy generated due to heat transfer. Because although Eq. (21) shows that increasing the Hartmann number leads to an increase in entropy, it should also be noted that increasing the Hartmann number leads to a decrease in velocity, which leads to a small effect of the magnetic field in total entropy generation. Increasing the Hartmann number and power-law index reduces the total entropy due to reduced heat transfer.

The variations of Bejan number are presented in Fig. 9. The Bejan number shows the ratio of the entropy generated due to the heat transfer to the total entropy generation. It can be seen that the Bejan number is almost constant for the shear-thickening fluid.

Because the effects of convection and variations in heat transfer are very small and the magnetic field has little effect. In the case of a shear thinning and Newtonian fluid, the Bejan number increases with increasing Hartmann number. It is true that increasing the Hartmann number reduces the entropy generated due to heat transfer (Fig. 8), but at the same time the entropy generation due to fluid friction decreases, which is more evident in the total entropy generated. Variations of the Bejan number become more obvious for shear-thinning fluid as the Hartmann number increases. Fig. 10 shows the contours of the streamlines, isotherms and total entropy generation in terms of the Hartmann number and the type of magnetic field applied. As can be seen, the change in the type of magnetic field applied becomes more apparent with the increasing Hartmann number. Applying a magnetic field as TMFA4 reduces the average Lorentz force applied to the fluid flow, which increases the strength and velocity of the fluid inside the cavity. Due to the fact that the magnetic field is applied against gravity, by applying the magnetic field uniformly, the center of the formed vortex tends upwards, while by applying a non-uniform magnetic field, the center of the vortex tends to the bottom of the cavity. The curvature and scattering of isotherms is greater in the non-uniform state of the magnetic field than in the uniform state. The total volumetric entropy generation is the same as heat transfer. It can also be seen from Fig. 10 that as the Hartmann number increases due to the decrease in gradients of temperature and velocity the total entropy generation decreases as shown in the Figure. According to Table 5, it can be seen that the strength of flow from TMFA1 to TMFA4 increases continuously, which is more tangible with increasing Hartmann numbers.

Table 4. Maximum values of streamlines (Ψ_{max}) at AR=2, Ra=10⁵, λ=90° and TMFA1

	λ=0				λ=90°			
	Ha=0	Ha=15	Ha=30	Ha=45	Ha=0	Ha=15	Ha=30	Ha=45
n=0.75	0.455	0.374	0.285	0.235	0.455	0.345	0.232	0.165
n=1.0	0.251	0.208	0.165	0.155	0.251	0.195	0.144	0.125
n=1.25	0.115	0.109	0.101	0.95	0.115	0.105	0.093	0.085

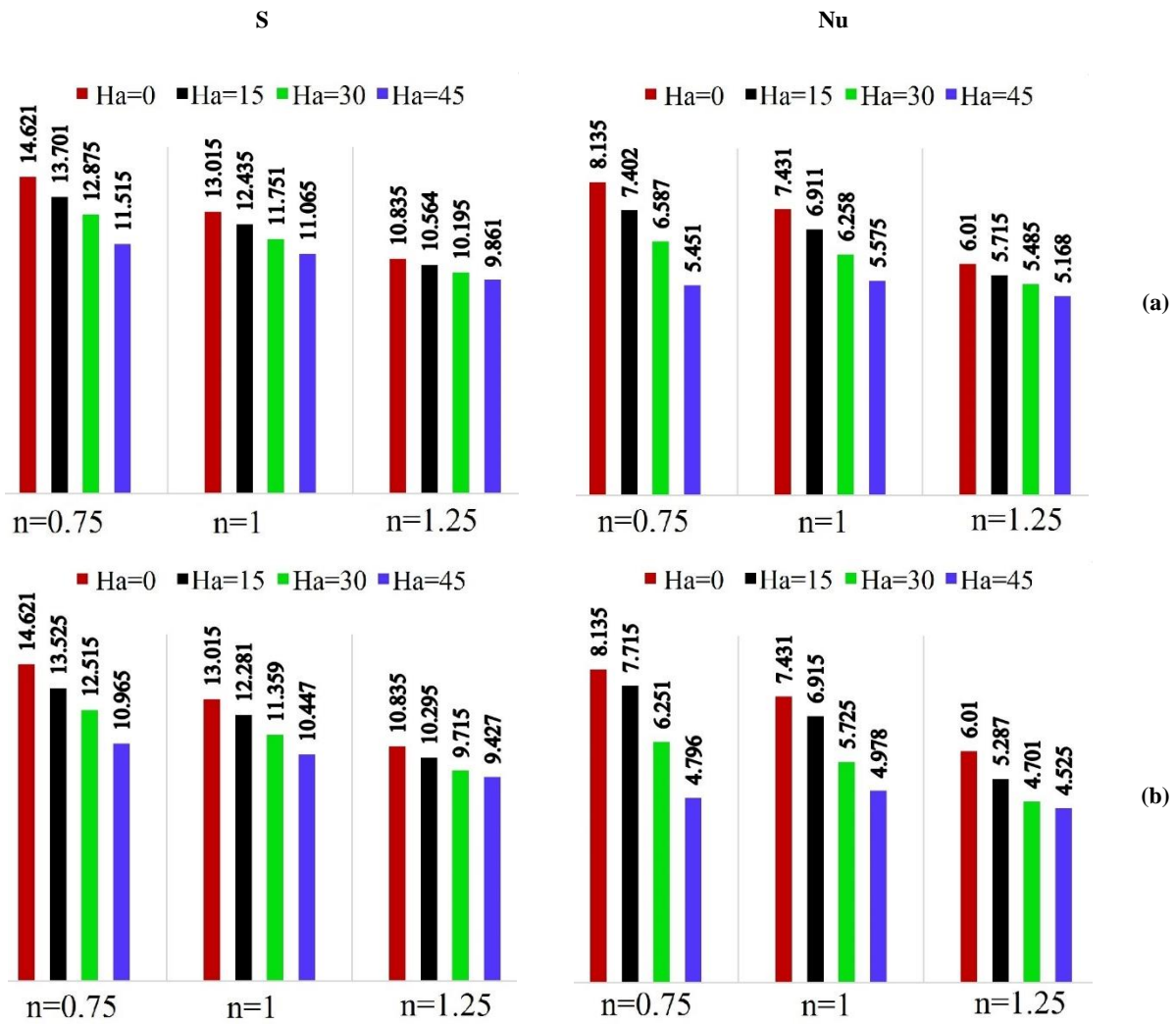


Fig. 8. Average Nusselt number and total entropy generation for variations of Hartmann number at AR=2, Ra=10⁵ and TMFA1 (a) $\lambda=0$ and (b) $\lambda=90^\circ$

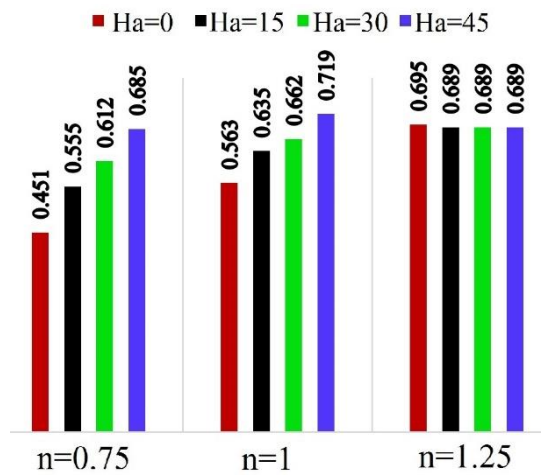


Fig. 9. Bejan number for variations of Hartmann number at AR=2, Ra=10⁵, $\lambda=90^\circ$ and TMFA1

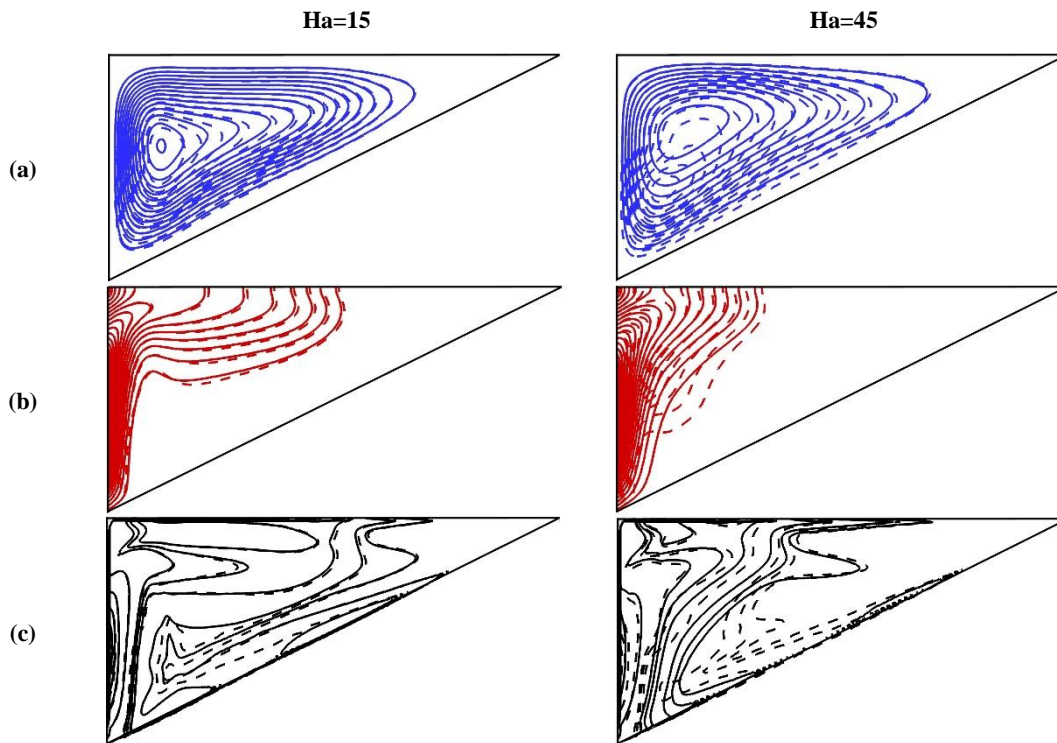


Fig. 10. Contours of (a) streamlines, (b) isotherms and (c) total entropy generation for various Hartmann numbers at AR=2, $n=1.0$, $\lambda=90^\circ$, TMFA1 (Continuous lines) and TMFA4 (Discontinuous lines)

Table 5. Maximum values of streamlines (Ψ_{max}) at AR=1, Ra=10⁵, $\lambda=0$ and $n=1.0$

	Ha=0	Ha=15	Ha=30	Ha=45
TMFA1	0.185	0.155	0.124	0.095
TMFA2	0.185	0.164	0.135	0.115
TMFA3	0.185	0.171	0.144	0.128
TMFA4	0.185	0.175	0.165	0.142

According to Fig. 11, the applied magnetic field uniformly results in the lowest velocity of the fluid flow. The non-uniform application of a magnetic field increases the velocity of the fluid, especially near walls, which increases the velocity and temperature gradients. Fig. 12 shows the average Nusselt number and the total entropy generation in terms of variations of the Hartmann number and the type of magnetic field applied. By changing the type of magnetic field applied from TMFA1 to TMFA4, the average Nusselt number and flow strength can be increased up to 25% and 50%, respectively. Increasing the Hartmann number from zero to 45 decreases the average Nusselt number by 25, 19, 14, and 6 percent for TMFA1 to TMFA4, respectively. The trend of variations in total entropy generation is similar to the average Nusselt number so the least changes has been seen for TMFA4. Fig. 13 shows

the simultaneous effect of the Hartmann and Rayleigh number on contours of streamlines, isotherms and total entropy generation. It is observed that by decreasing the Rayleigh number, the strength of fluid flow is reduced by up to 70%. Because by reducing the Rayleigh number, the effect of buoyancy forces is greatly reduced. Due to the isotherms, by decreasing the Rayleigh number, the curvature of the lines is reduced, which indicates the predominance of thermal conductivity. As the Rayleigh number decreases, entropy lines also behave like isotherms, indicating a decrease in entropy generation. Also, it can be seen that the effect of the Hartmann number decreases with the decrease of the Rayleigh number. The effect of the direction and strength of the magnetic field on the temperature profile for low Rayleigh numbers is negligible because in this state

thermal conductivity is dominant and the effects of convection are very small as shows in Fig. 14. Also, it can be seen in Rayleigh number 10^5 , the temperature is higher when the magnetic field is vertically applied, that indicating the heat transfer is higher. According to Fig. 15, it can be seen that in all Rayleigh numbers, increasing the Hartmann number decreases the average Nusselt number and the entropy generated, which this effect increases with increasing Rayleigh number. Applying a magnetic field in the form of horizontal for the Rayleigh numbers 10^3 , 10^4 and 10^5 leads to a decrease of 9, 13 and 38%, while for the vertical type it is 6, 10 and 23%.

It can be seen that the amount of entropy generation and the Nusselt number are a function of the Rayleigh number.

The Bejan number for variations of the Hartmann and Rayleigh number is tabulated in Table 6. It can be seen that the inverse relationship is established between the Bejan number and the Rayleigh numbers. Increasing the Rayleigh number increases the heat transfer and the entropy generated due to fluid friction due to the increased effects of fluid convection. At low Rayleigh numbers, the largest share of total entropy is related to heat transfer, while at high Rayleigh number this share decreases.

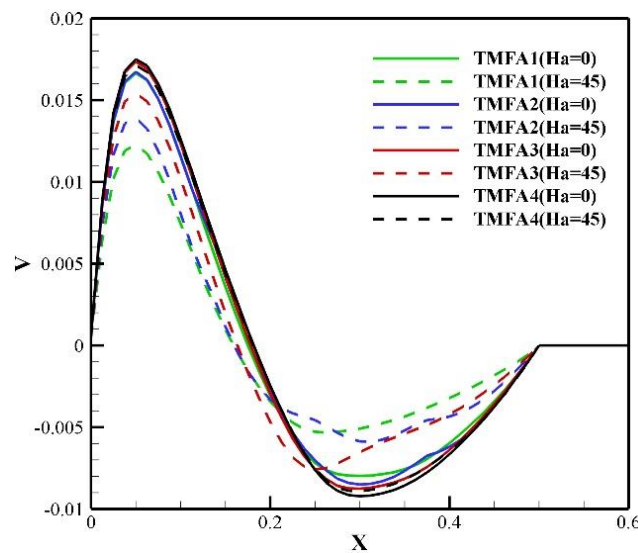


Fig. 11. Vertical velocity in $Y=0.375$ for variations of Hartmann number and TMFA at $AR=1$, $Ra=10^5$, $\lambda=0$ and $n=1.0$

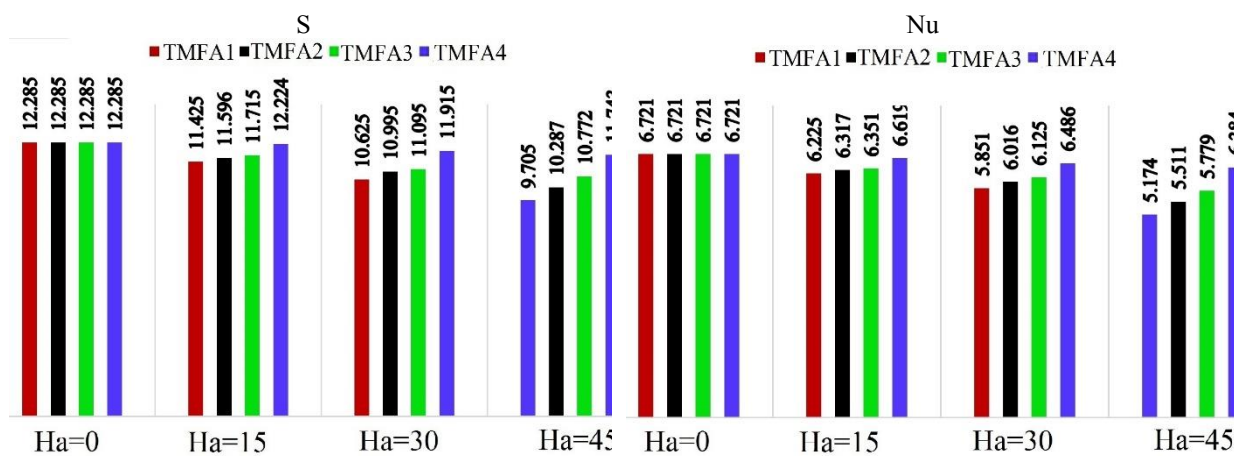


Fig. 12. Average Nusselt number and total entropy generation for variations of Hartmann number and TMFA at $AR=1$, $Ra=10^5$, $\lambda=0$ and $n=1.0$

5.2. Effect of Rayleigh number

Figure 16 shows the isotherms for the shear thinning and shear thickening fluid for different values of the Rayleigh numbers. It can be seen that at low Rayleigh numbers, the lines are more parallel to the hot wall that indicating the predominance of thermal

conductivity. The scattering and curvature of the lines increase with increasing Rayleigh numbers that indicating greater convection effects. Also, it can be seen that the effect of increasing the power-law index on reducing the dispersal of the lines increases with increasing the Rayleigh number.

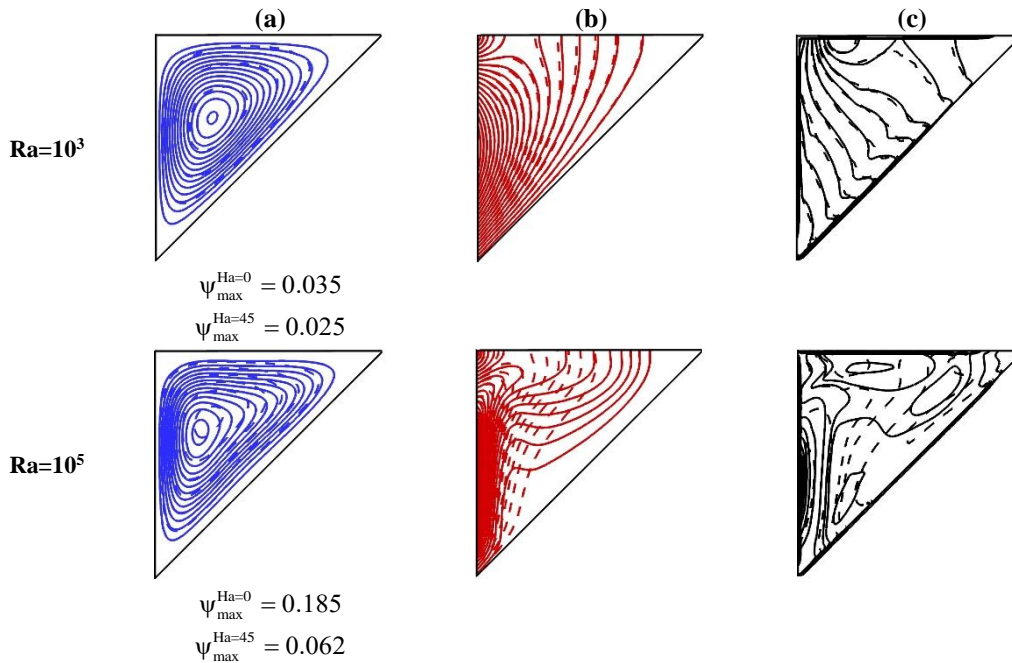


Fig. 13. Contours of (a) streamlines, (b) isotherms and (c) total entropy generation for various Rayleigh numbers at AR=1, n=1.0, λ=90°, TMFA1, Ha=0 (Continuous lines) and Ha=45 (Discontinuous lines)

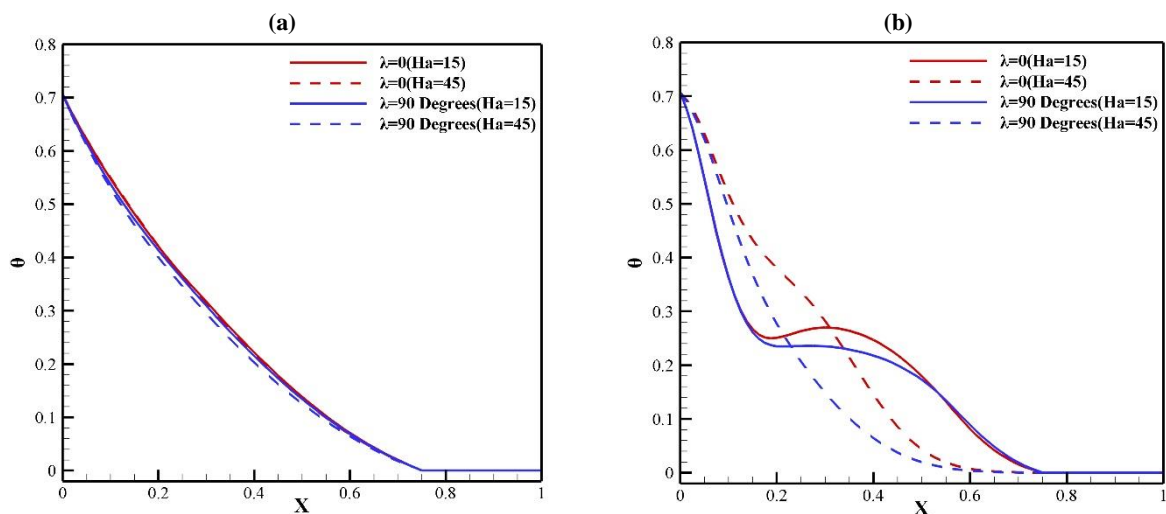


Fig. 14. Dimensionless temperature for variations of Hartmann number and angle of magnetic field applied at AR=1, TMFA1, n=1.0, (a) Ra=10³ and (b) Ra=10⁵

The temperature profile in the middle of the cavity for the different Rayleigh numbers values in the shear thinning, Newtonian and thickening fluid is shown in Fig. 17. Changing the temperature profile from linear to horizontal by increasing the Rayleigh number indicates a change in the heat transfer mechanism from conduction to convection. Also, in all Rayleigh numbers, the maximum and minimum temperatures are related to the shear thinning and shear thickening fluid, respectively, which in the same proportion to the amount of heat transfer changes. According to Fig. 18, it can be seen that increasing the power-law index from 0.75 to

1.25 for Rayleigh numbers 10^3 , 10^4 and 10^5 leads to a decrease of 15, 19 and 31% of the average Nusselt number, respectively. This trend of variations is observed for total entropy generation. At low Rayleigh numbers, due to the low convection effects and the predominance of thermal conductivity, the increase in fluid viscosity due to the increase in the power-law index has less effect. The Bejan number for variations of Rayleigh numbers and power-law index according to Table 6 shows that the share of heat transfer in entropy generation increases with increasing power-law index.

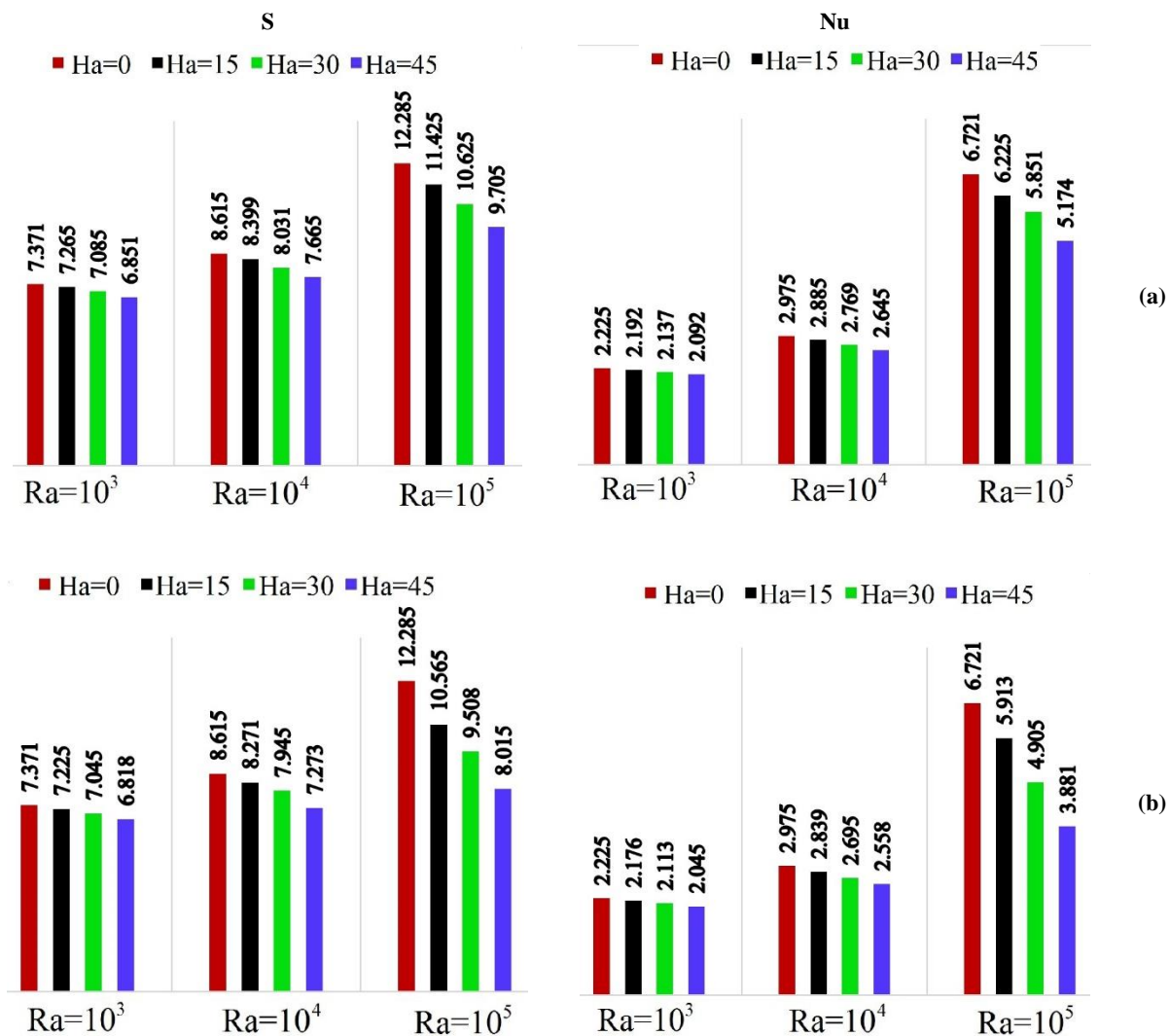


Fig. 15. Average Nusselt number and total entropy generation for variations of Hartmann number and Rayleigh number at AR=1, TMFA1, n=1.0, (a) $\lambda=0$ and (b) $\lambda=90^\circ$

The Bejan number also decreases with increasing Rayleigh number, because with increasing Rayleigh, the entropy due to fluid friction increases with increasing convection effects. According to Fig, 19, it is observed that with increasing the aspect ratio of the cavity, the movement space for the fluid flow increases and the flow strength more than doubles. The effect of the Rayleigh number is more evident as the aspect ratio increase. According to Fig, 20, in Rayleigh number 10^3 , because thermal conductivity is predominant, increasing the aspect ratio leads to decreasing the average Nusselt number, but for other Rayleigh numbers, increasing the aspect ratio leads to increasing the Nusselt number. Because with increasing the aspect ratio of the

cavity, the power of the convection increases. The highest entropy generation was observed in the highest aspect ratio and the highest Rayleigh number value. The effect of the type of magnetic field applied with variations of Rayleigh number is shown in Fig, 21. As can be seen, in low Rayleigh numbers, due to the predominance of thermal conductivity, the effect of the magnetic field is low and there is no significant difference between the different types of the magnetic field applied. This is very evident in the temperature profile. By changing the type of magnetic field applied from TMFA1 to TMFA4 for Rayleigh numbers 10^3 , 10^4 and 10^5 , respectively, the heat transfer rate can be increased by about 5, 11 and 23 percent.

Table 6. Bejan number for variations of Hartmann numbers and Rayleigh numbers at AR=1, TMFA1, $\lambda=90^\circ$ and $n=1.0$

		Ha=0	Ha=15	Ha=30	Ha=45
Ra=10 ³	Be	0.882	0.885	0.885	0.885
	$Be^* = \frac{Be_{Ra=10^3} - Be_{Ra=10^3}}{Be_{Ra=10^3}}$	0	0	0	0
Ra=10 ⁴	Be	0.783	0.795	0.805	0.805
	$Be^* = \frac{Be_{Ra=10^4} - Be_{Ra=10^3}}{Be_{Ra=10^3}}$	-11.2%	-10.2%	-5.8%	-5.8%
Ra=10 ⁵	Be	0.671	0.755	0.785	0.801
	$Be^* = \frac{Be_{Ra=10^5} - Be_{Ra=10^3}}{Be_{Ra=10^3}}$	-23.9%	-14.6%	-11.3%	-9.5%

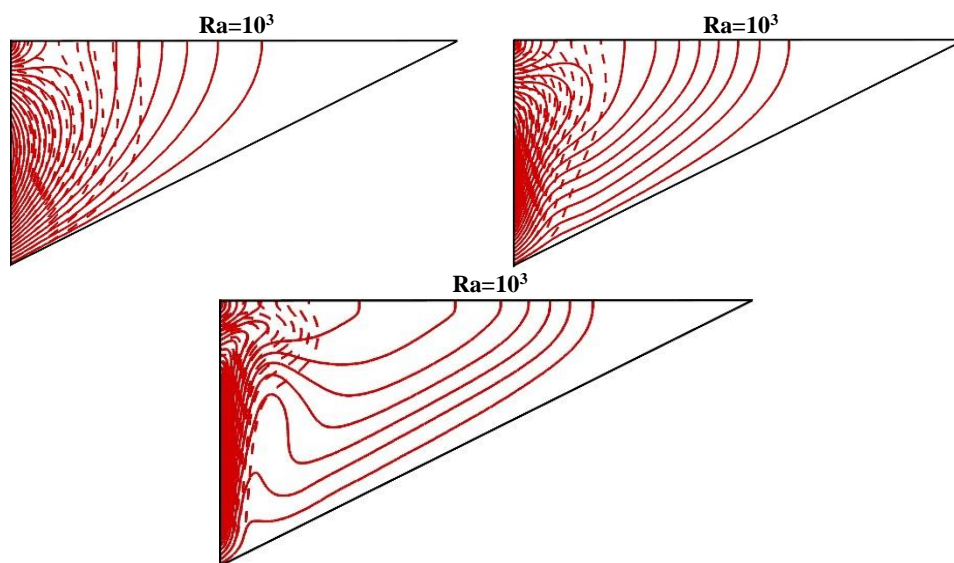


Fig. 16. Contours of isotherms for various Rayleigh numbers at AR=2, Ha=15, $\lambda=0$, TMFA1, $n=0.75$ (Continuous lines) and $n=1.25$ (Discontinuous lines)

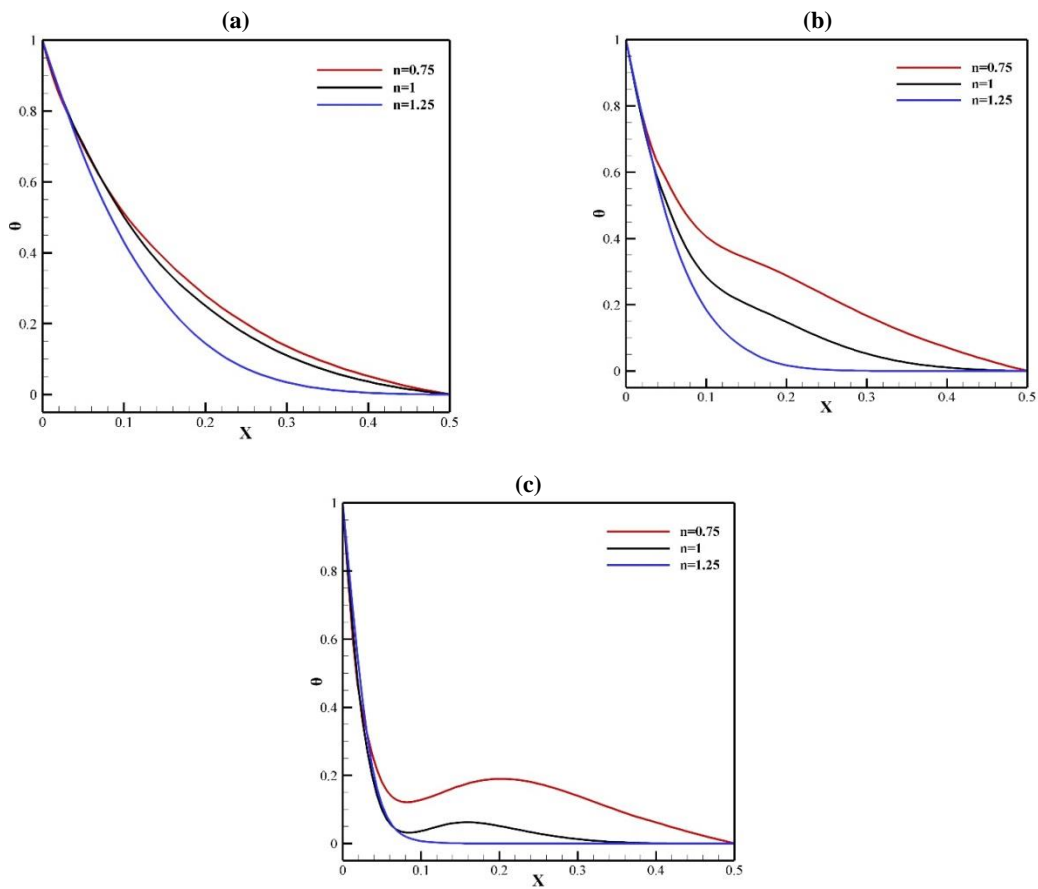


Fig. 17. Dimensionless temperature in $Y=0.675$ for variations of power-law index and Rayleigh numbers at $AR=2$, $TMFA1$, $Ha=15$, $\lambda=0$, (a) $Ra=10^3$, (b) $Ra=10^4$ and (c) $Ra=10^5$

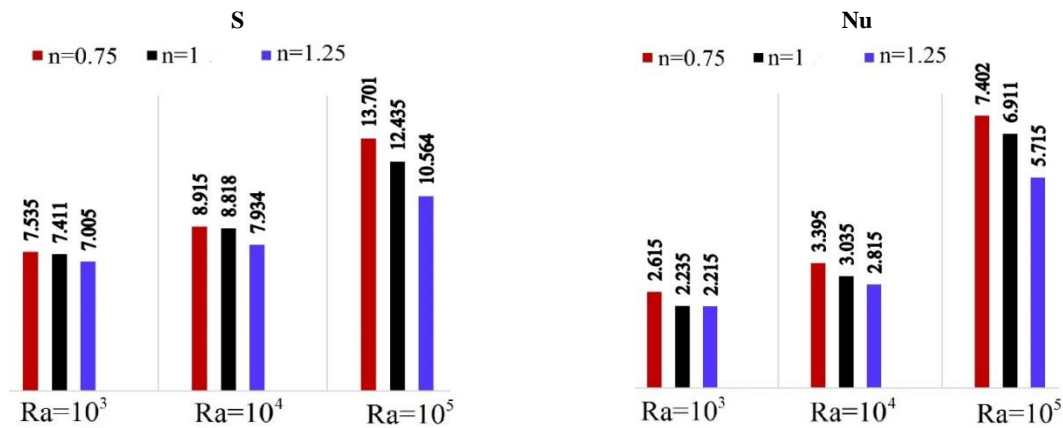


Fig. 18. Average Nusselt number and total entropy generation for variations of power-law index and Rayleigh numbers at $AR=2$, $TMFA1$, $Ha=15$ and $\lambda=0$

5.3. Effect of aspect ratio

Table 8 shows the maximum value of the streamlines for different values of the aspect ratio and the power-law index. It is observed that increasing the aspect ratio for the shear-thickening fluid has little effect on increasing

the created strength of the flow, while for the shear-thinning fluid this effect is much more pronounced. Increasing the aspect ratio increases the moving space of the fluid and the fluid flows more easily. According to Fig. 8 (b) and Fig. 22, it can be seen that in all values of power-law index and Hartmann

numbers, increasing the aspect ratio leads to increasing the average Nusselt number, which this effect decreases with increasing the power-law index. On average, increasing the aspect ratio from 0.5 to 2 leads to an increase of 25, 17 and 8% of the average Nusselt number for shear thinning, Newtonian and shear thickening fluid, respectively. Increasing the aspect ratio increases the convection effects and increases the cold wall surface for heat exchange. The effect of the

type of magnetic field applied to the shear thinning and shear thickening fluid for the aspect ratio of the cavity is shown in Fig. 23. It can be seen that for the shear thinning fluid, the change in the type of magnetic field applied from TMFA1 to TMFA4 Nusselt number increases by an average of 4, 10 and 14% for the aspect ratio of 0.5, 1 and 2, respectively, which this effect is for shear thickening fluid about 0, 3 and 6%.

Table 7. Bejan number for variations of power-law index and Rayleigh numbers at AR=2, TMFA1, Ha=15 and λ=0

		n=0.75	n=1.0	n=1.25
Ra=10 ³	Be	0.685	0.688	0.691
	$Be^* = \frac{Be_{Ra=10^3} - Be_{Ra=10^3}}{Be_{Ra=10^3}}$	0	0	0
Ra=10 ⁴	Be	0.625	0.648	0.675
	$Be^* = \frac{Be_{Ra=10^4} - Be_{Ra=10^3}}{Be_{Ra=10^3}}$	-8.7%	-5.8%	-2.3%
Ra=10 ⁵	Be	0.581	0.641	0.668
	$Be^* = \frac{Be_{Ra=10^5} - Be_{Ra=10^3}}{Be_{Ra=10^3}}$	-15.2%	-6.8%	-3.3%

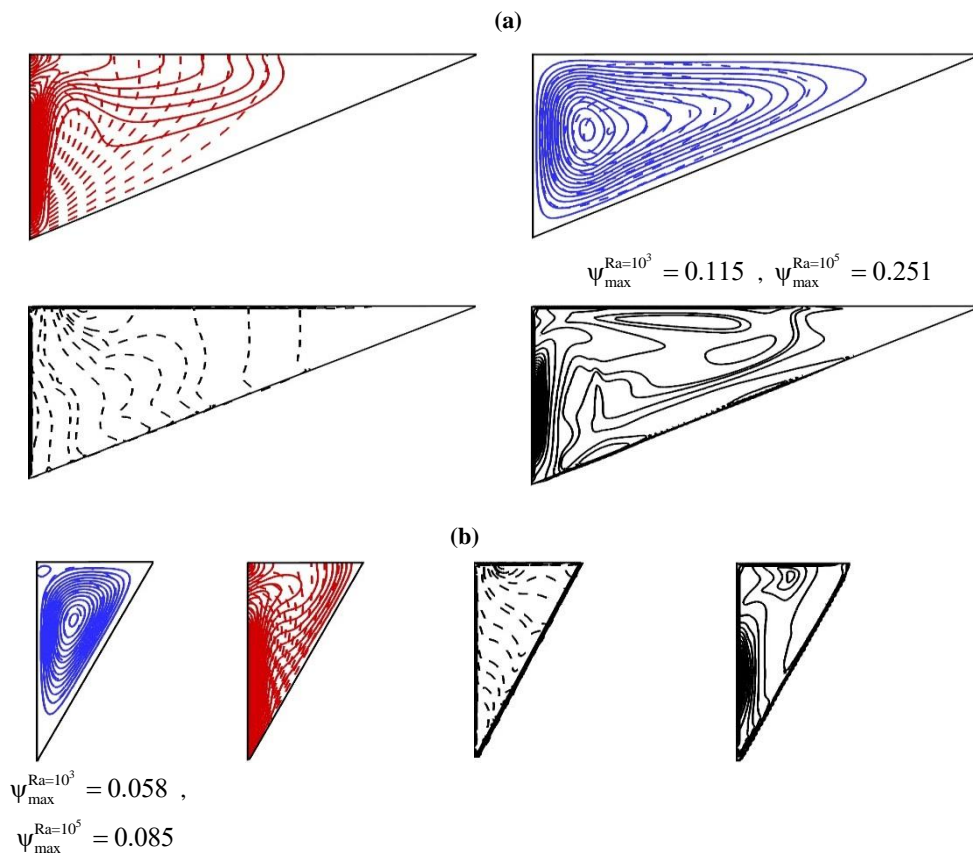


Fig. 19. Contours of streamlines (blue lines), isotherms (red lines) and total entropy generation (black lines) for various aspect ratio and Rayleigh numbers at n=1.0, Ha=0, Ra=10³ (Discontinuous lines), Ra=10⁵ (Continuous lines) (a) AR=2 and (b) AR=0.5

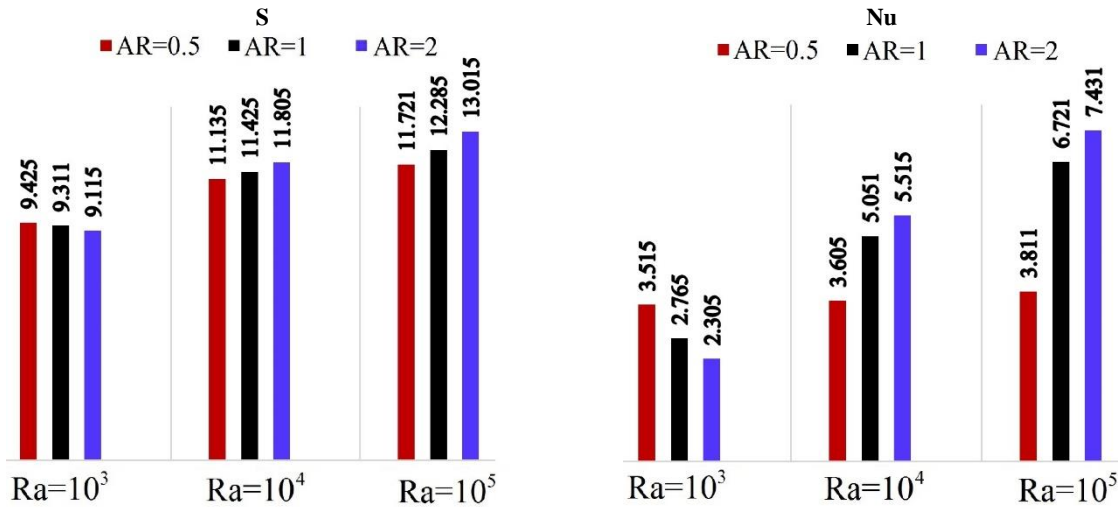


Fig. 20. Average Nusselt number and total entropy generation for variations of aspect ratio and Rayleigh numbers at $n=1.0$ and $Ha=0$

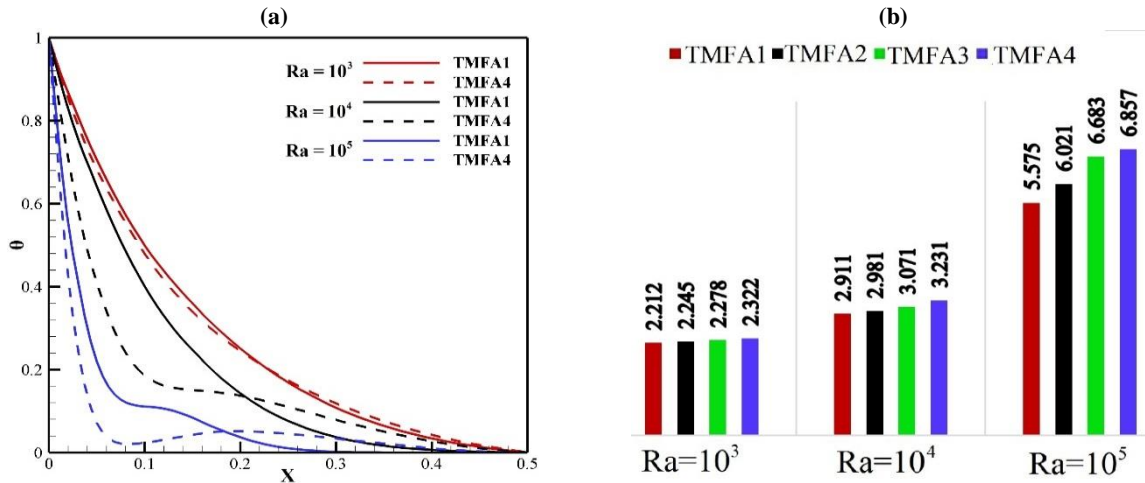


Fig. 21. (a) Dimensionless temperature in $Y=0.5$ and (b) Average Nusselt number for variations of Rayleigh numbers and type of magnetic field at $AR=2$, $n=1.0$, $Ha=45$ and $\lambda=0$

Table 8. Maximum values of streamlines (Ψ_{max}) at $Ra=10^5$ and $Ha=0$

	$n=0.75$	$n=1.0$	$n=1.25$
AR=0.5	0.108	0.085	0.0725
AR=1	0.275	0.185	0.125
AR=2	0.455	0.251	0.135

6. Conclusion

The aim of this study was to investigate the heat transfer and entropy generated by the natural convection of Newtonian and non-Newtonian fluids in two types of shear thinning and shear thickening fluids inside a triangular cavity with variable aspect ratio. The magnetic field was applied to the cavity in 4 different shapes, horizontally and vertically,

and the simulation was performed by writing computer code in Fortran language using the multiple relaxation time lattice Boltzmann method. The accuracy of the obtained results was confirmed in comparison with the studies of different references. The effect of Rayleigh number, Hartmann number, type and angle of the magnetic field applied, power-law index and aspect ratio of the cavity was investigated. The most important results are:

1- In all cases, increasing the Hartmann number decreases the flow velocity that leading to a decrease in the flow strength and the average Nusselt number. On average, this effect is about 25% greater for shear-thinning fluid than for shear-thickening fluid.

2- The angle and type of magnetic field applied are very important parameters in controlling the amount of heat transfer and can be used to achieve flows with desired strength. Applying a magnetic field horizontally creates a flow with less strength and for this reason, it also results in a lower average Nusselt number. Applying a uniform magnetic field compared to another type of applied leads to a greater reduction in heat transfer and flow strength.

3- Increasing the fluid power-law index caused increases the viscosity of the fluid flow and reduces the ease of fluid movement, which reduces the strength of flow and the amount of heat transfer so that thermal conductivity is the predominant heat transfer phenomenon for the shear-thickening fluid. Due to the low convection effects for the shear thickening fluid, the effect of the angle and type of magnetic field applied is much less compared to Newtonian and shear thinning fluid.

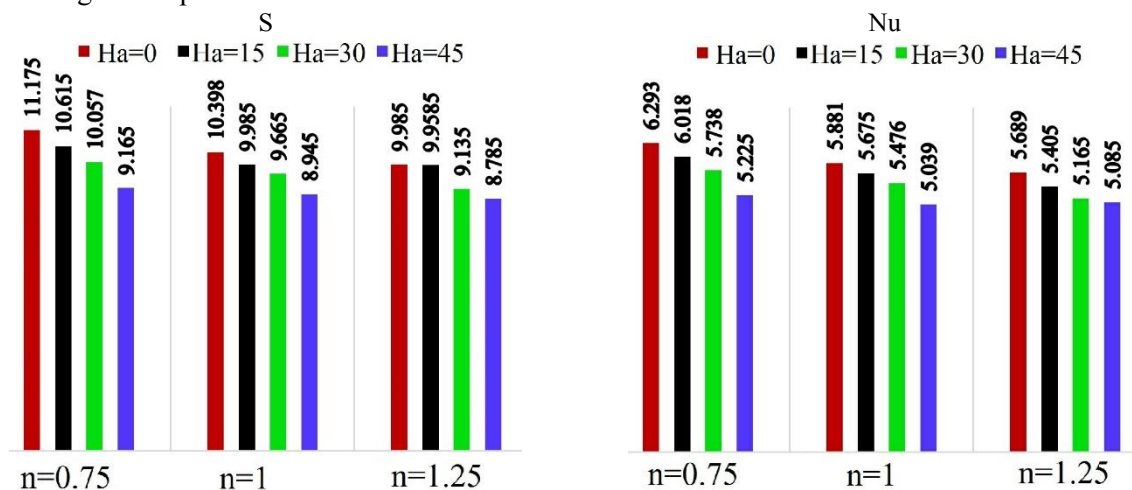
4- Increasing the aspect ratio of the cavity increases the space of motion of the fluid and leads to the formation of vortices with more power. More heat transfer and an increase in the effect of the magnetic field are observed by increasing the aspect ratio. The effect of the

type and angle of the magnetic field applied is more obvious with increasing the aspect ratio of the cavity. Increasing the aspect ratio is not very effective for the shear-thickening fluid.

5- The Rayleigh number variable can be used to achieve more powerful currents and increase heat transfer. Thermal conductivity is the predominant phenomenon in low Rayleigh numbers, which results in the lowest heat transfer rate. Increasing the Rayleigh number due to the increase in buoyancy forces increases the effect of the magnetic field, the aspect ratio of the cavity, and the power-law index.

6- Based on the obtained results, it was observed that the total volumetric entropy generation increases with increasing Hartmann number, Rayleigh number and aspect ratio and decreasing power-law index of fluid. Except for the $Ra=10^5$, shear thinning fluid, $AR=2$ and absence of magnetic field ($Be = 0.451$), in other cases it can be seen that $Be > 0.5$, meaning that the heat transfer has the largest share in the entropy generated. The lowest amount of Bejan number is related to the shear thickening fluid and decreasing the Rayleigh number leads to increasing the Bejan number.

7- Using this numerical study, a comprehensive view can be obtained of the design of heat transfer devices and equipment inside shaped cavities and it can be understood under what conditions the rate of irreversibility is minimal.



(a)

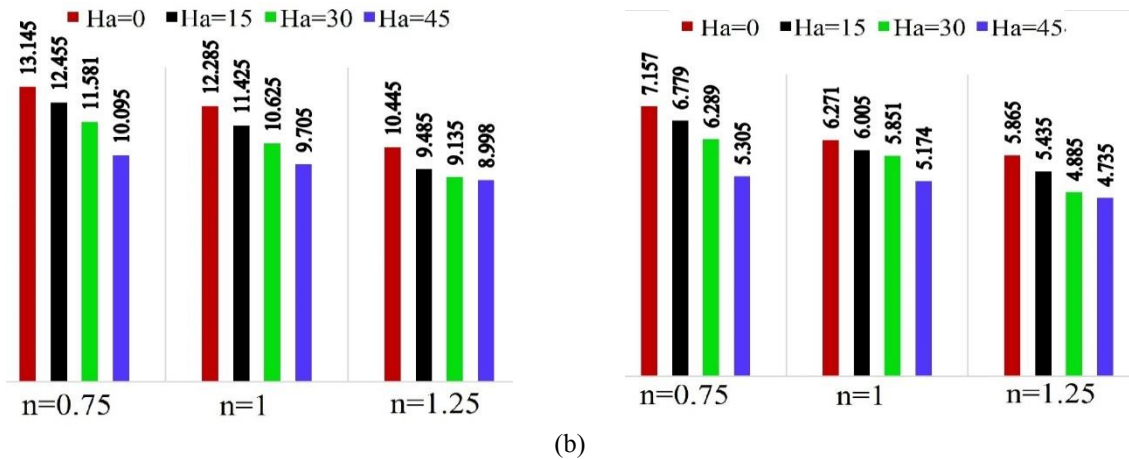


Fig. 22. Average Nusselt number and total entropy generation for variations of Hartmann number at $Ra=10^5$, $TMFA1$, $\lambda=90^\circ$, (a) $AR=0.5$ and (b) $AR=1$

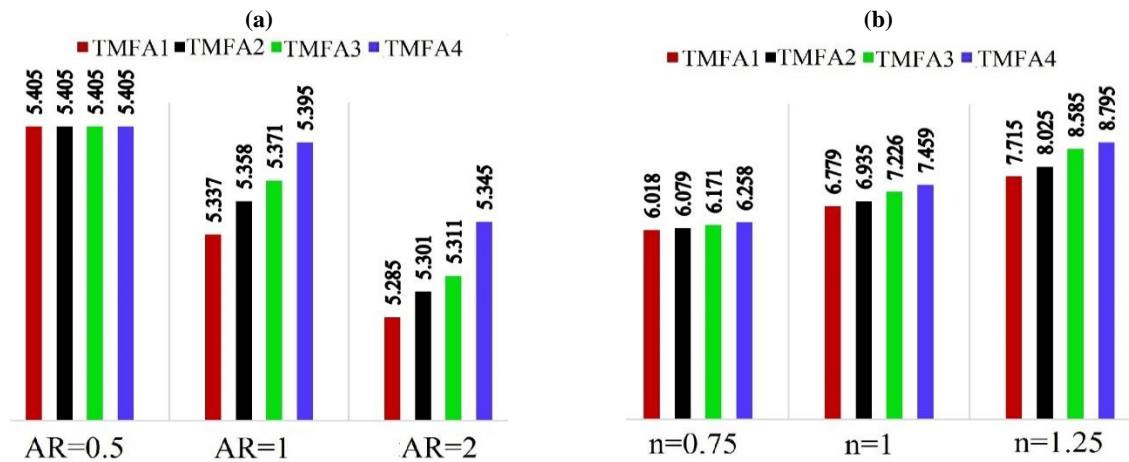


Fig. 23. Average Nusselt number for variations of aspect ratio and power-law index at $Ra=10^5$, $Ha=45$, $\lambda=0$, (a) $AR=0.5$ and (b) $AR=2$

References

- [1] Aziz T, Javaid S, Aziz A, Sadiq MA. Group theoretical analysis for magnetohydrodynamic generalized Stokes' flow and radiative heat transfer model of a non-Newtonian nanofluid with heat generation/absorption. *Journal of Thermal Analysis and Calorimetry*. 2021 Jan;143:985-1002.
- [2] Mortuja Sarkar G, Sahoo B. Dual solutions of a magnetohydrodynamic stagnation point flow of a non-Newtonian fluid over a shrinking sheet and a linear temporal stability analysis. *Proceedings of the Institution of Mechanical Engineers, Part E: Journal of Process Mechanical Engineering*. 2021 Apr;235(2):527-35.
- [3] Murthy MK. Numerical investigation on magnetohydrodynamics flow of Casson fluid over a deformable porous layer with slip conditions. *Indian Journal of Physics*. 2020 Dec;94(12):2023-2032.
- [4] Mohamed RA, Hady FM, Mahdy A, Abozai OA. Laminar MHD natural convection flow due to non-Newtonian nanofluid with dust nanoparticles around an isothermal sphere: Non-similar solution. *Physica Scripta*. 2021 Jan 11;96(3):035215.
- [5] Dimitrienko YI, Li S. Numerical simulation of MHD natural convection heat transfer in a square cavity filled with Carreau fluids under magnetic fields in different directions. *Computational and Applied Mathematics*. 2020 Dec;39(4):1-26.

- [6] Idowu AS, Falodun BO. Effects of thermophoresis, Soret-Dufour on heat and mass transfer flow of magnetohydrodynamics non-Newtonian nanofluid over an inclined plate. Arab Journal of Basic and Applied Sciences. 2020 Jan 1;27(1):149-165.
- [7] Toghraie D. Numerical simulation on MHD mixed convection of Cu-water nanofluid in a trapezoidal lid-driven cavity. International Journal of Applied Electromagnetics and Mechanics. 2020 Jan 1;62(4):683-710.
- [8] Kefayati GH, Tang H. Simulation of natural convection and entropy generation of MHD non-Newtonian nanofluid in a cavity using Buongiorno's mathematical model. International Journal of Hydrogen Energy. 2017 Jul 6;42(27):17284-327.
- [9] Izadi M, Sheremet MA, Mehryan SA. Natural convection of a hybrid nanofluid affected by an inclined periodic magnetic field within a porous medium. Chinese Journal of Physics. 2020 Jun 1;65:447-58.
- [10] Nemati M, Mohamadzade H, Sefid M. Investigation the Effect of Direction of Wall Movement on Mixed Convection in Porous Enclosure with Heat Absorption/Generation and Magnetic Field. Fluid Mechanics & Aerodynamics Journal. 2020 Jun 21;9(1):99-115.
- [11] Daneshpour M, Rafee R. Determination of the diameter ratios for minimum entropy generation in a borehole geothermal heat exchangers using numerical simulation of the flow and heat transfer. Journal of Solid and Fluid Mechanics. 2016 Mar 20;6(1):249-58.
- [12] Opanuga AA, Adesanya SO, Okagbue HI, Agboola OO. Impact of Hall current on the entropy generation of radiative MHD mixed convection casson fluid. International Journal of Applied and Computational Mathematics. 2020 Apr;6(2):1-8.
- [13] Ijaz Khan M, Alzahrani F. Numerical simulation for the mixed convective flow of non-Newtonian fluid with activation energy and entropy generation. Mathematical Methods in the Applied Sciences. 2021 Jun;44(9):7766-7777.
- [14] Shehzad SA, Madhu M, Shashikumar NS, Gireesha BJ, Mahanthesh B. Thermal and entropy generation of non-Newtonian magneto-Carreau fluid flow in microchannel. Journal of Thermal Analysis and Calorimetry. 2021 Feb;143(3):2717-2727.
- [15] Li Z, Shahsavari A, Niazi K, Al-Rashed AA, Talebizadehsardari P. The effects of vertical and horizontal sources on heat transfer and entropy generation in an inclined triangular enclosure filled with non-Newtonian fluid and subjected to magnetic field. Powder Technology. 2020 Mar 15;364:924-942.
- [16] Anitha S, Thomas T, Parthiban V, Pichumani M. Modeling of Newtonian and non-Newtonian-based coolants for deployment in industrial length-scale shell and tube heat exchanger. International Journal of Modern Physics C (IJMPC). 2021;32(06):1-24.
- [17] Mallawi FO, Bhuvaneshwari M, Sivasankaran S, Eswaramoorthi S. Impact of double-stratification on convective flow of a non-Newtonian liquid in a Riga plate with Cattaneo-Christov double-flux and thermal radiation. Ain Shams Engineering Journal. 2021 Mar 1;12(1):969-81.
- [18] Waqas M, Khan WA, Asghar Z. An improved double diffusion analysis of non-Newtonian chemically reactive fluid in frames of variables properties. International Communications in Heat and Mass Transfer. 2020 Jun 1;115:104524.
- [19] Qiao Y, Zeng Y, Ding Y, Fan J, Luo K, Zhu T. Numerical simulation of two-phase non-Newtonian blood flow with fluid-structure interaction in aortic dissection. Computer methods in biomechanics and biomedical engineering. 2019 Apr 26;22(6):620-630.
- [20] Abugattas C, Aguirre A, Castillo E, Cruchaga M. Numerical study of bifurcation blood flows using three different non-Newtonian constitutive models. Applied Mathematical Modelling. 2020 Dec 1;88:529-49.
- [21] Lu G, Wang XD, Duan YY. A critical review of dynamic wetting by complex fluids: from Newtonian fluids to non-Newtonian fluids and nanofluids. Advances in colloid and interface science. 2016 Oct 1;236:43-62.

- [22] Kashyap D, Dass AK, Oztop HF, Abu-Hamdeh N. Multiple-relaxation-time lattice Boltzmann analysis of entropy generation in a hot-block-inserted square cavity for different Prandtl numbers. *International Journal of Thermal Sciences*. 2021 Jul 1;165:106948.
- [23] Aly AM, Raizah ZA. Incompressible smoothed particle hydrodynamics simulation of natural convection in a nanofluid-filled complex wavy porous cavity with inner solid particles. *Physica A: Statistical Mechanics and its Applications*. 2020 Jan 1;537:122623.
- [24] Kazemian Y, Esfahani JA, Fanaee SA. Simulation of combustion flowfield in porous media with lattice Boltzmann method. *Journal of Thermophysics and Heat Transfer*. 2020 Jul;34(3):591-600.
- [25] Sato K, Koshimura S. Validation of the MRT-LBM for three-dimensional free-surface flows: an investigation of the weak compressibility in dam-break benchmarks. *Coastal Engineering Journal*. 2020 Jan 2;62(1):53-68.
- [26] Cheng PX, Gui N, Yang XT, Tu JY, Jiang SY, Jia HJ. Liutex-based analysis of drag force and vortex in two-phase flow past 2-D square obstacle using LBM on GPU. *Journal of Hydrodynamics*. 2020 Oct;32(5):820-833.
- [27] Rahman A, Nag P, Molla MM, Hassan S. Magnetic field effects on natural convection and entropy generation of non-Newtonian fluids using multiple-relaxation-time lattice Boltzmann method. *International Journal of Modern Physics C*. 2021 Jan 17;32(01):2150015.
- [28] Jahanbakhshi A, Nadooshan AA, Bayareh M. Magnetic field effects on natural convection flow of a non-Newtonian fluid in an L-shaped enclosure. *Journal of Thermal Analysis and Calorimetry*. 2018 Sep;133(3):1407-16.
- [29] Afsana S, Molla MM, Nag P, Saha LK, Siddiq S. MHD natural convection and entropy generation of non-Newtonian ferrofluid in a wavy enclosure. *International Journal of Mechanical Sciences*. 2021 May 15;198:106350.
- [30] Zhang R, Aghakhani S, Pordanjani AH, Vahedi SM, Shahsavari A, Afrand M. Investigation of the entropy generation during natural convection of Newtonian and non-Newtonian fluids inside the L-shaped cavity subjected to magnetic field: application of lattice Boltzmann method. *The European Physical Journal Plus*. 2020 Feb 1;135(2):184.
- [31] Rahimi A, Sepehr M, Lariche MJ, Mesbah M, Kasaeipoor A, Malekshah EH. Analysis of natural convection in nanofluid-filled H-shaped cavity by entropy generation and heatline visualization using lattice Boltzmann method. *Physica E: Low-Dimensional Systems and Nanostructures*. 2018 Mar 1;97:347-62.
- [32] Abdel-Nour Z, Aissa A, Mebarek-Oudina F, Rashad AM, Ali HM, Sahnoun M, El Ganaoui M. Magnetohydrodynamic natural convection of hybrid nanofluid in a porous enclosure: numerical analysis of the entropy generation. *Journal of Thermal Analysis and Calorimetry*. 2020 Sep;141(5):1981-1992.
- [33] Bhowmick D, Randive PR, Pati S, Agrawal H, Kumar A, Kumar P. Natural convection heat transfer and entropy generation from a heated cylinder of different geometry in an enclosure with non-uniform temperature distribution on the walls. *Journal of Thermal Analysis and Calorimetry*. 2020 Jul;141(2):839-857.
- [34] Li Y, Firouzi M, Karimipour A, Afrand M. Effect of an inclined partition with constant thermal conductivity on natural convection and entropy generation of a nanofluid under magnetic field inside an inclined enclosure: applicable for electronic cooling. *Advanced Powder Technology*. 2020 Feb 1;31(2):645-657.
- [35] Trouette B. Lattice Boltzmann simulations of a time-dependent natural convection problem. *Computers & Mathematics with Applications*. 2013 Nov 1;66(8):1360-71.
- [36] Nemati, M., Sefid, M., Mohamadzade, H., "The effect of wall shape and aspect ratio on heat transfer non-Newtonian power law fluid in the presence of magnetic field", *Iranian J Mech Eng Trans ISME*, Vol. 22(4), pp. 116-130, 2021.
- [37] He Q, Li Y, Huang W, Hu Y, Li D, Wang Y. Lattice Boltzmann model for dense suspended particles based on improved bounce-back method. *Computers &*

- Mathematics with Applications. 2020 Aug 1;80(3):552-567.
- [38] He B, Lu S, Gao D, Chen W, Lin F. Lattice Boltzmann simulation of double diffusive natural convection in heterogeneously porous media of a fluid with temperature-dependent viscosity. Chinese Journal of Physics. 2020 Feb 1;63:186-200.
- [39] Ilis GG, Mobedi M, Sunden B. Effect of aspect ratio on entropy generation in a rectangular cavity with differentially heated vertical walls. International Communications in Heat and Mass Transfer. 2008 Jul 1;35(6):696-703.
- [40] Khezzar L, Siginer D, Vinogradov I. Natural convection of power law fluids in inclined cavities. International Journal of Thermal Sciences. 2012 Mar 1;53:8-17.
- [41] Kefayati GR. Mesoscopic simulation of magnetic field effect on natural convection of power-law fluids in a partially heated cavity. Chemical Engineering Research and Design. 2015 Feb 1;94:337-354.